

Department of Biomedical Sciences
University of Veterinary Medicine Vienna

Institute of Pharmacology and Toxicology
(Head: Univ.-Prof. Dr.med.univ. Veronika Sexl)

Detection of Primary and Secondary Radicals during Antileishmanial Action of Endoperoxides

Bachelor thesis submitted for the fulfilment of the requirements for the degree of
Bachelor of Science (BSc.)

University of Veterinary Medicine Vienna

submitted by
Lara Näglein

Vienna, June 2020

All experiments for this thesis were conducted from February to May 2020 in the group and under the supervision of Ao. Univ.-Prof. Dr.rer.nat. Lars Gille at the Institute of Pharmacology and Toxicology in the Department of Biomedical Sciences.

Reviewer: Dipl.-Biol. Dr.rer.nat. Catharina Duvigneau

University of Veterinary Medicine Vienna

Department of Biomedical Sciences

Institute for Medical Biochemistry

Veterinärplatz 1

1210 Vienna

Acknowledgements

First of all, I would like to wholeheartedly thank my supervisor Ao.Univ.-Prof. Dr.rer.nat. Lars Gille for giving me the opportunity to conduct this thesis and, especially, for supporting me during the whole working process. He supported me whenever help was needed and assisted me through his advice, encouragement and, in particular, with his endless patience. Although the last months happened to be more complicated than initially expected due to the current external circumstances, he enormously contributed to the realization of my thesis. Thank you incredibly much for your support; I could not wish for a better supervisor.

Furthermore, I want to express my gratitude to Ao.Univ.-Profⁱⁿ Drⁱⁿ rer.nat Katrin Staniek and Nikola Knoll who supported me throughout my thesis and created a great working atmosphere.

I sincerely thank Mag. Gerald Geroldinger, PhD and Larissa Schölzky for reading my thesis and providing me with constructive and valuable advice on how to improve my work.

Moreover, I want to thank Drⁱⁿ Silke Näglein for always supporting me and having faith in me throughout my studies. Without her encouragement I would not be where I am today.

Last but not least, I acknowledge the financial support for this work by the Austrian Science Fund (FWF) under grant P 27814-B22.

Table of content

1. Introduction.....	1
1.1. Leishmaniasis	1
1.2. <i>Leishmania</i>	2
1.2.1. Life cycle.....	2
1.2.2. Host-parasite interaction	3
1.3. <i>Leishmania</i> epidemiology	4
1.3.1. Mediterranean Region	5
1.3.2. European Region.....	6
1.3.3. Canine leishmaniasis	6
1.4. Antileishmanial drugs	6
1.4.1. Pentavalent antimonials.....	6
1.4.2. Amphotericin B	7
1.4.3. Miltefosine	8
1.4.4. Paromomycin.....	8
1.4.5. Sitamaquine.....	8
1.4.6. Pentamidine.....	9
1.4.7. Combination therapy.....	9
1.5. Endoperoxides	10
1.6. Susceptibility of <i>Leishmania</i> to (endo-) peroxides.....	10
1.7. Artemisinin as antimalarial drug.....	12
1.8. Primary and secondary radicals	14
1.9. Electron paramagnetic resonance (EPR) spectroscopy.....	15
1.10. Spin trapping	16
1.11. Spin traps	17
1.12. Problems for spin traps in cells.....	19
1.13. Primary radicals of endoperoxides	20

1.14. Aims of the current project.....	21
2. Materials and methods.....	23
2.1. Chemicals	23
2.2. Cell culture of <i>Leishmania</i>	24
2.3. Viability assays.....	24
2.3.1. Viability assays with single compounds.....	25
2.3.2. Combined viability assays with compounds and inhibitors	25
2.4. EPR spectroscopy.....	26
2.4.1. Spin trapping in the biomimetic system	26
2.4.2. Spin trapping in the biological system (LtP)	27
2.4.3. Extraction and spin trapping of lipid-derived radicals.....	28
2.5. Simulation and data analysis	29
3. Results	30
3.1. Influence of EPs on viability of LtP	30
3.2. Detection of radicals triggered by H ₂ O ₂ and EPs	31
3.2.1. Spin trapping in biomimetic systems	31
3.2.1.1. H ₂ O ₂ -derived radicals in water	32
3.2.1.2. H ₂ O ₂ -derived radicals in PBS	35
3.2.1.3. Asc-derived radicals in water	36
3.2.1.4. Asc-derived radicals in PBS	40
3.2.1.5. Art-derived radicals in water	42
3.2.1.6. Art-derived radicals in PBS.....	46
3.2.2. Spin trapping of EP-derived radicals in LtP	47
3.2.2.1. Asc-derived radicals in LtP	47
3.2.2.2. Art-derived radicals in LtP	51
3.2.3. Spin trapping of lipid-derived radicals in LtP and model systems	52
4. Discussion	58

4.1. Drugs against leishmaniasis	58
4.2. EPs against leishmaniasis	58
4.3. Activation of Asc and Art	58
4.4. Basic mechanism of EPs and experimental evidence	59
4.4.1. Biomimetic system: H ₂ O ₂	60
4.4.2. Biomimetic system: Asc	60
4.4.3. Biomimetic system: Art	61
4.4.4. Biological system (LtP): Asc and Art	61
4.5. Extraction of lipid-derived spin adducts	61
4.6. Practical conclusion	63
4.7. General conclusions	63
5. Summary	65
6. Zusammenfassung	66
7. Abbreviations	68
8. References	71
9. List of figures	77
10. List of tables	80

1. Introduction

1.1. Leishmaniasis

Leishmaniasis is a neglected vector borne-disease with a high burden in developing countries. According to the World Health Organization (WHO) it is one of the seven most important tropical diseases. It is endemic especially in tropical and subtropical countries and is caused by different species of protozoan parasites of the genus *Leishmania*. The disease is transmitted to humans by a bite of a female sand fly and depends on the distribution of this vector (Torres-Guerrero et al. 2017).

Leishmaniasis has a worldwide distribution and is found in 89 countries. There are about 1.5 to 2 million new cases and 70.000 deaths per year due to this disease. Depending on the species of *Leishmania* different clinical manifestations can occur (Torres-Guerrero et al. 2017).

The different clinical manifestations, which are caused by the different species of *Leishmania*, are shown in Tab. 1 (Kaye and Scott 2011).

The most severe form of leishmaniasis, which accounts for up to 70,000 deaths per year, is visceral leishmaniasis or kala-azar caused by *L. infantum* and *L. donovani*. In this disease, internal organs, such as the liver, spleen and bone marrow are affected. Other *Leishmania spp.* are responsible for cutaneous, mucocutaneous or diffuse cutaneous leishmaniasis. They are chronic, slow-to-heal diseases and their symptoms are limited to the skin or mucosal surface. Cutaneous leishmaniasis is characterized by a local swelling and a papule appear on the skin. The diffuse cutaneous form shows a lack of cellular immune response to parasite antigens, which results in the spreading through tissue, blood or lymph pathways and, therefore, in the development of lesions of the skin. The invasion at mucocutaneous leishmaniasis happens slowly and sometimes with no initial disturbance, which allows the mucosal injury to remain undetected. Sometimes it causes only low local swelling and usually it starts in the nasal mucosa and then spreads to the oral mucosa. For a correct diagnosis, it is important to take biopsies as a diagnostic material and to identify the species of *Leishmania* (Kaye and Scott 2011, Torres-Guerrero et al. 2017).

Tab. 1: The most relevant species of human-pathogenic *Leishmania* and corresponding clinical manifestations, categorized by geographic occurrence and subgenus (Kaye and Scott 2011).

MAIN DISEASE MANIFESTATION	SPECIES
New World, subgenus <i>Leishmania</i>	
visceral leishmaniasis	<i>L. infantum</i>
cutaneous leishmaniasis	<i>L. infantum, L. mexicana, L. pifanol and L. amazonensis</i>
diffuse cutaneous leishmaniasis	<i>L. mexicana and L. amazonensis</i>
New World, subgenus <i>Viannia</i>	
cutaneous leishmaniasis	<i>L. braziliensis, L. guyanensis, L. panamensis and L. peruviana</i>
mucocutaneous leishmaniasis	<i>L. braziliensis and L. panamensis</i>
Old World, subgenus <i>Leishmania</i>	
visceral leishmaniasis	<i>L. donovani and L. infantum</i>
cutaneous leishmaniasis	<i>L. major, L. tropica and L. aethiopica</i>
diffuse cutaneous leishmaniasis	<i>L. aethiopica</i>

1.2. *Leishmania*

Leishmania are protozoal parasites that undergo a multistage life cycle characterized by transmission between the sand fly as their transmission vector and humans or other mammals as their final hosts. In the Old World (Africa, Asia and Europe) the parasites are spread by sand flies of the genus *Phlebotomus* and in the New World (North and South America, Oceania) by the genus *Lutzomyia*. *Leishmania* have two different morphologies during their life cycle, namely promastigotes and amastigotes. Promastigotes are flagellated and motile cells, which are found in the sand fly. There they undergo many stages of differentiation until they become non-dividing infectious cells, which are transmitted during the sand fly's bite. The intracellular parasites, which live in the phagolysosomes inside the macrophages of their final host and do not have a flagellum, are called amastigotes (Kaye and Scott 2011, Wheeler et al. 2011, Torres-Guerrero et al. 2017).

1.2.1. Life cycle

The detailed life cycle of *Leishmania* is shown in Fig. 1. During the bite of a sand fly of an infected host, amastigotes are taken up by the sand fly and converted to procyclic promastigotes in the midgut of the sand fly. These procyclic promastigotes are the first stage

of the parasite inside the vector and represent a slightly motile form, which replicates in the insect's midgut. Then they differentiate into infective, non-dividing metacyclic promastigotes, which are ready for transmission and are deposited in the skin of a new mammalian host. Upon biting the potential host, the sand fly transmits metacyclic promastigotes together with immunomodulatory parasite-derived proteophosphoglycans and salivary components to avoid blood coagulation. The promastigotes are phagocytosed by the cells of the local environment, such as tissue-resident macrophages, dermal dendritic cells or neutrophils and after reaching their intracellular residence they are transformed into amastigotes. These amastigotes replicate in their host cells and if they reach a critical number, the host cells rupture, which leads to a reinfection of local phagocytes. The life cycle becomes closed when another sand fly bites the infected host and takes up the amastigotes (Bates 2007, Kaye and Scott 2011).

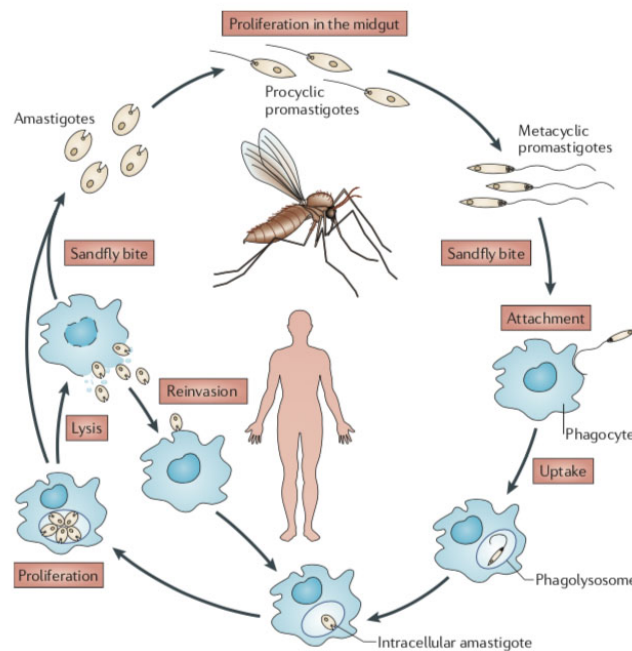


Fig. 1: Lifecycle of *Leishmania* parasites with sand flies as vectors and humans as mammalian hosts (Kaye and Scott 2011).

1.2.2. Host-parasite interaction

Leishmania are intracellular parasites, residing inside vacuoles in macrophages or dermal dendritic cells - the so-called phagolysosomes. Their survival in the phagolysosome depends on various host-parasite interactions. *Leishmania* are different from other phagocytosed

components because they are able to actively modulate their uptake into macrophages and transform from promastigotes to amastigotes including a profound change in morphology and metabolism. Moreover, the amastigotes can replicate inside the phagolysosome of their host macrophages. The parasite organism has developed many mechanisms for an effective uptake into macrophages and regulates the conditions inside the phagolysosomes to be more suitable for its growth and to avoid its destruction. Since the macrophage defense, such as antigen presentation, immune activation and apoptosis, is compromised, it is less destructive for the parasites. Especially the *Leishmania* survival factors, for example, the zinc-dependent metalloprotease GP63, the lipophosphoglycan (LPG) or inhibitors of serine peptidase (ISP) are responsible for these changes. GP63 is expressed by promastigotes, cleaves multiple host proteins and directly interacts with the complement component C3b taken up into cells. LPG is a surface glycolipid of promastigotes, which contains side chains that trigger the immune response in macrophages. ISP inhibits host enzymes, like the neutrophil elastase, trypsin or chymotrypsin and prevents the action of the host protein kinase PKR. Due to these mechanisms, the parasite can adapt to its environment and counteracts host defense (Podinovskaia and Descoteaux 2015).

Many *Leishmania* spp., therefore, may cause mild symptom long-term parasitism, which possibly leads to a non-protective increase of the immune response and, consequently, to tissue damage. The first interaction of *Leishmania* promastigotes with the host macrophages occurs via the flagellum of the parasite. After that intracellular survival factors are released by the parasite and the regulation of the macrophage's phagocytic activity is modulated. In this process many macrophagal pathways are targeted by *Leishmania* to reduce infection-induced inflammation, for instance, the inflammatory response with the production of interleukin 12 (IL-12), IL-17 and IL-6. These few examples may highlight the complexity of this host-parasite interaction (Rotureau et al. 2009, Podinovskaia and Descoteaux 2015).

1.3. *Leishmania* epidemiology

Leishmaniasis exists in all continents except Antarctica and Oceania and is considered as the third most common parasitic disease (Bethony et al. 2011). Leishmaniasis is a disease typically found in tropical and subtropical regions. However, global warming may extend the endemic region of the sand fly vector and, therefore, the spread of the disease (World Health Organization 2018).

The burden of visceral leishmaniasis spreads out among regions, even so alone the African and South-East Asia regions contribute 30 % of the worldwide cases of visceral leishmaniasis (World Health Organization 2019).

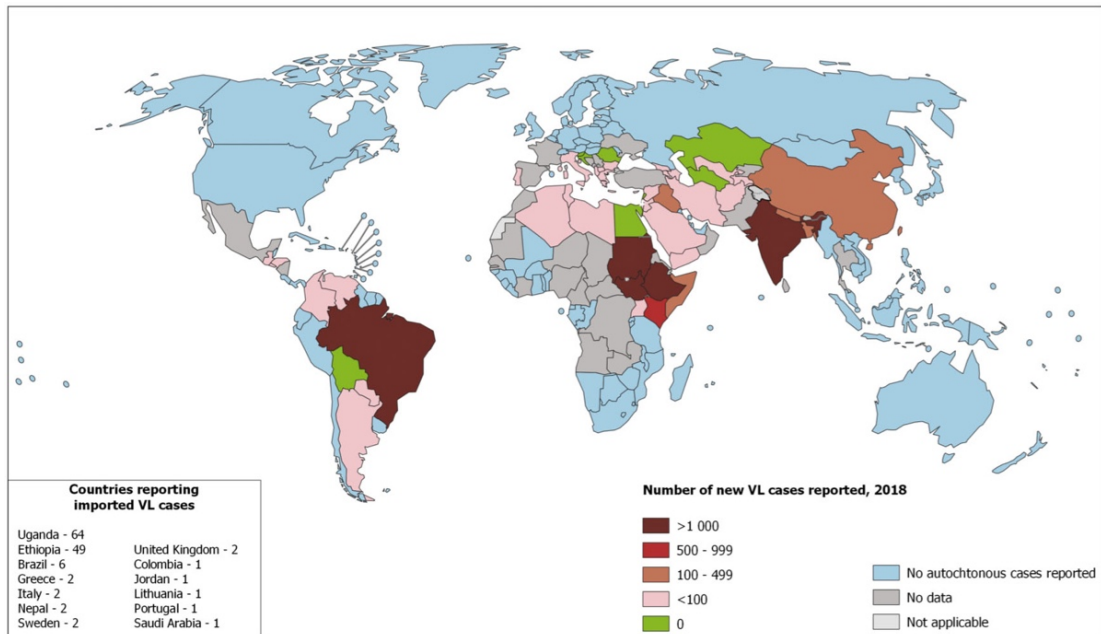


Fig. 2: Worldwide distribution of cases of visceral leishmaniasis in 2018. Modified after (World Health Organization 2018).

Exemplary, Fig. 2 shows the worldwide distribution of visceral leishmaniasis in 2018. The majority of new cases of visceral leishmaniasis was reported in Brazil, India, Kenya and Ethiopia. Import of leishmaniasis is also an important point contributing to the spread of the disease. Especially Uganda and Ethiopia were the countries with the most reported cases of visceral leishmaniasis imported (World Health Organization 2018).

1.3.1. Mediterranean Region

In the Mediterranean Region, leishmaniasis is an important disease. Cutaneous and visceral leishmaniasis are very present. There are two categories of leishmaniasis in dependence of their reservoir host, anthroponotic and zoonotic leishmaniasis. The hosts of anthroponotic leishmaniasis, caused by *L. tropica*, are humans. Zoonotic leishmaniasis is caused by *L. major* and wild or domestic animals are their hosts. Both forms are endemic in this region and 69.6 % of the total number of cutaneous leishmaniasis cases detected worldwide in 2016 occurred in the Mediterranean Region (World Health Organization 2019).

1.3.2. European Region

In the European Region, zoonotic, as well as anthroponotic cutaneous leishmaniasis, are endemic and found in 25 countries. Visceral leishmaniasis is mostly reported by 27 countries with dogs, foxes, gerbils and jackals as their main reservoir host. Especially canine leishmaniasis, a form of zoonotic leishmaniasis, poses a major problem (World Health Organization 2019).

1.3.3. Canine leishmaniasis

Dogs often carry *Leishmania* parasites, especially of the species *L. infantum*. Canine leishmaniasis is a progressive and chronic disease with different clinical outcomes. It can manifest as an asymptomatic infection, a cutaneous form or a life-threatening generalized visceral disease affecting skin, lymphatic organs and the hematopoietic system. It is endemic in about 70 countries all around the world. Due to climate change, the disease is spreading geographically towards the north also in Europe. These changes influence the habitat of the sand flies and the disease gets a seasonal pattern according to local climate (Ferroglio et al. 2005, Karkamo et al. 2014).

1.4. Antileishmanial drugs

Leishmania parasites directly influence the host's immune system because they affect macrophages and other cells of the mononuclear phagocytic system. Due to their intracellular location, it is very difficult to find active substances to fight this infection. There are some antileishmanial compounds available for the different forms of the disease, but even well-established therapeutics can result in severe side effects, lack of efficacy or high costs. Some substances vary in their activity against different *Leishmania* species. In addition, *Leishmania* show resistances against some established therapeutics. Therefore, there is a great need for developing new drugs to treat the infection (Zulfiqar et al. 2017).

1.4.1. Pentavalent antimonials

Pentavalent antimonials were the first drugs against leishmaniasis. They are still used as chemotherapeutics, but the resistance development to this drug in *Leishmania* is increasing. They were especially used in therapies for visceral and cutaneous leishmaniasis under different conditions. Pentavalent antimonials act as a pro-drug and are converted into trivalent antimonite, which is the active form of the drug. The reduction of this drug takes place in the macrophages or directly in the parasites. Especially the reduction of antimonial pro-drugs in parasites is a possible resistance mechanism. If this activity in parasites

declines, antimonials are less activated leading to drug resistance. The antimonials kill *Leishmania* spp. by DNA fragmentation, inhibition of glycolysis and via several other metabolic pathways. The high resistance against pentavalent antimonials results from the widespread misuse of the drugs, for example, due to underdosing or uncompleted therapy cycles (Singh et al. 2012).

For cutaneous leishmaniasis the WHO recommends a local therapy with an intralésional infiltration, which should be performed every five to seven days for two to five times. Benefits of this therapy are the low dosage, lower systemic side effects, rapid action and high drug concentrations in the lesion (Ghorbani and Farhoudi 2018).

The systemic usage of pentavalent antimonials is limited because of their cardio-, nephro- and hepatotoxicity, and, therefore, alternative drugs should be considered (Ghorbani and Farhoudi 2018).

1.4.2. Amphotericin B

In areas with a high antimonial resistance, the polyene antifungal drug amphotericin B (AmB) is widely used. Although AmB has a high efficiency against *Leishmania*, it can cause severe nephrotoxicity, thrombophlebitis and hypokalemia. Ergosterol, the main sterol of the leishmanial cell membrane is the primary target of AmB. Furthermore, AmB complexes cholesterol of host macrophages and thereby inhibits the binding of *Leishmania* promastigotes to macrophages and their internalization. At higher concentration levels aqueous pores are induced in the leishmanial cell membrane, which results in osmotic changes and consequently, cell lysis (Singh et al. 2012).

To treat systemic infections, AmB has to be injected intravenously because it has a very low bioavailability upon oral administration. Moreover, it is insoluble in aqueous media and, therefore, mixed with deoxycholate micelles in pharmaceutical formulations. Because these micelles are unstable, AmB gets released into the bloodstream and is transferred to lipoproteins, which then are absorbed by host cells, including macrophages and kidney cells. The success of AmB treatment mostly depends on the patient's immunity status and its impairment by other diseases, such as HIV (Singh et al. 2012, Ghorbani and Farhoudi 2018).

Due to the toxicity of AmB, there is another pharmaceutical formulation where deoxycholate has been replaced by lipids. This lipid formulation, the liposomal AmB, maintains its antifungal activity, shows very high efficacy to cure the disease and is less toxic. Furthermore, it circulates in the body for a long time and penetrates the tissues efficiently

because of its small size. In visceral leishmaniasis liposomal AmB has been proven as a drug with more than 95 % efficacy, but its high costs limit the usage (Singh et al. 2012, Ghorbani and Farhoudi 2018).

1.4.3. Miltefosine

Miltefosine is the first oral drug against visceral leishmaniasis with a high antileishmanial activity. It is an alkyl phosphocholine compound developed for anticancer therapy. It is often utilized in combination with liposomal AmB. Typical side effects of miltefosine are hepatotoxicity, nephrotoxicity and teratogenicity, which limit its use during pregnancy. Miltefosine reduces the lipid content and enhances the phosphatidylethanolamine content of the cell membrane in promastigotes. These mechanisms were suggested to cause inhibition of phosphatidylethanolamine-N-methyltransferase and may contribute to a decreased parasite proliferation. Additionally, miltefosine inhibits the AKT/PKB signaling pathway in infected host cells, which is essential for cell survival. So far, no resistance to miltefosine was reported. However, in some patients a relapse after nine to twelve months was observed. The typical duration of treatment is 28 days, but this value can differ between countries (Singh et al. 2012, Ghorbani and Farhoudi 2018).

1.4.4. Paromomycin

Paromomycin is an aminoglycoside antibiotic with antileishmanial and antibacterial activity. It was used to cure visceral and cutaneous leishmaniasis. Studies show a high efficacy and excellent tolerability for paromomycin like AmB. Paromomycin has a great potential as a topical therapy for cutaneous leishmaniasis and is easy to apply. However, it is rather expensive. Typical side effects of this drug are ototoxicity and nephrotoxicity. Its mechanism is not fully understood, but it has been shown that cationic paromomycin binds to the glycocalyx of *Leishmania*, facilitating its uptake. Inside *Leishmania* the primary target of paromomycin is the mitochondrion. In parallel, it inhibits leishmanial protein synthesis. Due to its limited use, no drug resistance during patient treatment was observed so far (Singh et al. 2012).

1.4.5. Sitamaquine

Sitamaquine is an 8-aminoquinoline and was developed for the treatment of visceral leishmaniasis. Studies in patients show a high efficacy of this drug. A great advantage of this compound is that it can be administered orally. Sitamaquine has some side effects like vomiting, dyspepsia, cyanosis, nephritic syndrome, abdominal pain and headache. *In vitro*,

this drug influences the motility, morphology and growth of the parasites. Electrostatic interactions between anionic polar phospholipid head groups and positively charged sitamaquine take place and, consequently, interactions with phospholipid acyl chains lead to drug insertion into biological membranes provoking pore formation with subsequent ion leakage and osmotic stress. Although the actual target of sitamaquine is still discussed, it was shown that inhibition of mitochondrial complex II could be involved. Resistance against this drug has not been reported until now, but more studies are required to understand the exact mode of action and its toxicity (Dueñas-Romero et al. 2007, Carvalho et al. 2011, Singh et al. 2012).

1.4.6. Pentamidine

Pentamidine is an aromatic diamine, which is mainly used for the treatment of visceral leishmaniasis. It is injected intramuscularly and enters *Leishmania* promastigotes through arginine and polyamine transporters. Its exact mechanism of action is not fully understood, but it was shown to enhance the efficacy of mitochondrial respiratory chain complex II inhibitors and decrease mitochondrial membrane potential. The efficacy of pentamidine is limited by various side effects, such as nephrotoxicity, hypoglycemia, myocarditis and hypotension. Although resistance for this drug was observed, its mechanism is not well understood (Singh et al. 2012).

1.4.7. Combination therapy

The benefit of monotherapeutic treatments is often limited by various adverse effects or resistance development. Therefore, combination therapies with different antileishmanial drugs are an option. Many studies demonstrate that an antileishmanial drug increases its pharmacological effects when it is combined with another drug. The combination often allows to lower the doses of the individual drugs resulting in toxicity reduction and less side effects. Furthermore, often the duration of the treatment can be shortened and the resistance of *Leishmania* can be prevented. Two examples for successful combination therapies are miltefosine with AmB and miltefosine with liposomal AmB. A study of Ghorbani and Farhoudi showed that miltefosine activity was enhanced when it was combined with AmB and, therefore, the treatment duration was reduced, which also leads to decreased therapy costs. Another study demonstrated that miltefosine together with a single injection of liposomal AmB leads to a reduced treatment duration from 28 to seven days without a decrease in drug efficacy (Dorlo et al. 2012, Ghorbani and Farhoudi 2018).

1.5. Endoperoxides

Peroxides are substances characterized by a peroxide group (O-O). The simplest peroxide is hydrogen peroxide (H₂O₂) in which each oxygen atom of the O-O group is linked to a hydrogen atom. There are also many other types of peroxides in the human body. These organic peroxides have their peroxide bridge between two carbon atoms or one carbon atom and one hydrogen atom. Organic peroxides can arise from the reaction of carbon-centered radicals with oxygen. On the other hand, endoperoxides (EP) have their peroxide group between two carbon atoms of a heterocycle. Endogenous EPs are intermediates of the prostaglandin biosynthesis. They are products of the cyclooxygenases that are converting arachidonic acid into a variety of prostanoid lipid mediators. These mediators are important in physiological regulation processes and inflammation. Organic hydroperoxides or EPs form highly reactive oxygen-centered radicals after one-electron reduction. In living cells electron donors for this reduction of peroxides are redox-active transition metals, like iron (Fe²⁺) and copper (Cu⁺) (Ricciotti and Fitzgerald 2011, Fudickar and Linker 2018).

1.6. Susceptibility of *Leishmania* to (endo-) peroxides

Aerobic organisms can cope with normal levels of reactive oxygen species (ROS), which arise from various intracellular sources including small amounts of free Fe²⁺. Mammalian cells have mechanisms for oxidative defense including chemical, enzymatic and genetic processes and, therefore, only excessive amounts of ROS cause pathologies. Additionally, host cells can detoxify ROS/peroxides and microorganisms have their own defense system (Mitra and Andrews 2013). Because of that, ROS/peroxides are not the first choice for new pharmacological treatments. Only specific types of peroxides, for example EPs have demonstrated a pharmacological benefit as a treatment against intracellular protozoal pathogens, like the well-known artemisinin (Art) against *Plasmodia* parasites, which reside inside erythrocytes (Tang et al. 2004, Baptista and Wainwright 2011).

There are many differences between *Plasmodia* and *Leishmania*, but both are dependent on the iron/heme supply by their mammalian host cells. These pathogens are specifically susceptible to peroxides, because free iron, which is mostly part of the labile iron pool (LIP) is a trigger for oxidative stress. For example, the benefit of hydroperoxides as a treatment against intracellular protozoal parasites is limited, because these peroxides are detoxified by the mammalian host cells. Therefore, EPs are more suitable, because they partially can escape from this defense system and are lipophilic, which enables them to cross cell

membranes. In mammalian cells highly specific EPs exist only temporarily during the prostaglandin synthesis of prostaglandin G₂ and H₂. Thus, these compounds are less targeted by the host antioxidative defense system (Kakhlon and Cabantchik 2002, Mitra and Andrews 2013). To achieve their pharmacological function via radical formation, EPs have to be activated by single electron reduction (Dong and Vennerstrom 2003).

Previous studies showed that for the treatment of cutaneous leishmaniasis in a mouse model the EP ascaridole (Asc) is effective. For the activation of Asc in *Leishmania* the LIP could be the major source and, therefore, studies about the total cellular metal concentrations in *Leishmania* and their host cells were made. For these studies *Leishmania tarentolae* promastigotes (LtP) as a parasitic model and a J774 macrophage cell line as host cells were chosen. The results of the total metal concentrations in LtP and J774 cells are shown in Tab. 2. The concentration of total cellular iron, which includes various forms (for example, Fe in the LIP or protein-bound iron), is about 511 μM in J774 cells. This is only about half of the concentration present in LtP (Geroldinger et al. 2017).

Tab. 2: Total concentrations for selected metals in LtP and J774 cells (Geroldinger et al. 2017).

Metal	LtP (μM)	J774 (μM)
Fe	1161 \pm 350	511 \pm 53
Cu	83 \pm 55	67 \pm 14
Mn	359 \pm 197	23 \pm 1

Tab. 3 shows that 41 % of total iron are in the LIP of LtP and 62 % of the LIP are Fe²⁺ which are, therefore, available for the cleavage of EPs. The results for J774 cells are shown in Tab. 2 and reveal that the total iron concentration is only about 44 % of the iron concentration, which is present in LtP. Furthermore, Tab. 4 shows that 17 μM Fe²⁺ of the LIP are available in the J774 for reaction. This is only about 6 % of the Fe²⁺ concentration which is available in LtP for the reaction with EPs (Geroldinger et al. 2017).

Tab. 3: Iron concentrations in LtP (Geroldinger et al. 2017).

Compartment	Type	Fe (μM)
LtP, whole cell	total Fe	1161 \pm 350
LIP in LtP	Fe ²⁺ and Fe ³⁺	481 \pm 75
Fe (II) in LtP	Fe ²⁺	298 \pm 89

Tab. 4: Iron concentrations in J774 cells (unpublished data).

Compartment	Type	Fe (μM)
J774 cell	total Fe	511
LIP in J774	Fe ²⁺ and Fe ³⁺	21
Fe (II) in J774	Fe ²⁺	17

The higher Fe²⁺ concentrations in LIP of *Leishmania* than in J774 cells are an indicator for the higher susceptibility with respect to EPs and, therefore, their function as potential antileishmanial agents (Geroldinger et al. 2017).

1.7. Artemisinin as antimalarial drug

Art is a secondary plant metabolite which is a sesquiterpene lactone with an EP group. The EP Art is used for clinical treatment of malaria, caused by the most pathogenic human malaria parasite *Plasmodium falciparum*. The generation of highly reactive carbon-centered radicals by cleavage of the EP bridge in Art was shown to be essential for its pharmacological activity. *Plasmodium falciparum* resides in human erythrocytes in the parasitophorous vacuole (Robert et al. 2005, Manske et al. 2012).

There, the major iron source for Art activation is heme, which is derived from the parasite's heme biosynthesis and the hemoglobin digestion, as shown in Fig. 3. Because of the hemoglobin digestion by the parasites, high levels of heme are released and can react with Art to form radicals. Therefore, Art shows a high efficacy in killing *Plasmodia* with a minimum of side effects on the healthy erythrocytes (Wang et al. 2015).

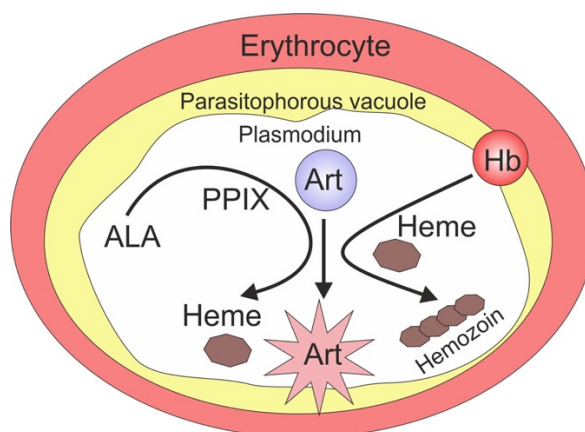


Fig. 3: Activation of artemisinin (Art) in *Plasmodium falciparum*, which resides in the parasitophorous vacuole of human erythrocytes. The mechanism relies on heme, generated in the parasite from the heme biosynthesis and hemoglobin digestion. During the hemoglobin digestion heme is released, which accumulates in crystalline pigmented particles, called hemozoin (ALA = δ -aminolevulinic acid, Hb = hemoglobin, PPIX = protoporphyrin IX). Modified after (Wang et al. 2015).

The two activation pathways of Art in *Plasmodia*, which are shown in Fig. 3, vary between the different parasite stages. During the early ring stage, the activation of Art relies mainly on the heme biosynthesis. Studies showed that the level of activation at that stage is rather low, because the heme production of the parasite at this early stage is at a low level. When the parasite reaches later stages both activation pathways are included in the heme production, but the hemoglobin digestion plays the major role in the activation of Art. The more heme is released from the parasite the higher is the Art activity. Hence Art is exponentially potent against the *Plasmodia* parasite inside erythrocytes. Art also shows a selective toxicity towards the parasite because it is only activated in infected erythrocytes, which makes it a suitable drug to treat malaria (Wang et al. 2015).

In the past, various Art derivatives were established, which show activity against *Plasmodia* and other parasites. For instance, artemisone and its thiomorpholine precursor artemiside beyond their activity against *Plasmodium falciparum* showed activity against *Toxoplasma gondii*. *In vivo* studies revealed that a treatment with the two derivatives controlled *Plasmodia* parasite replication. Therefore, the mice survived acute infection (Dunay et al. 2009).

Another example is artesunate, which is a semisynthetic analogue of Art. A study identified artesunate as a highly potent anti-lymphoma treatment option. Thereby artesunate suppresses growth in most B lymphoma cells and, comparable to anti-malaria treatments,

leaves normal B-cells unaffected. Moreover, in a xenograft model it inhibits highly aggressive tumor growth (Våtsveen et al. 2018).

1.8. Primary and secondary radicals

Upon activation of EPs by transition metals one-electron reduction of the O–O bridge is expected. This heterolytic cleavage leads to an oxygen-centered radical and an oxo anion. These oxygen-centered EP-derived radicals are highly unstable and often stabilized by rearrangement to carbon-centered radicals. These radicals and their peroxy products are the intermediates, which interact with cellular components. This leads to the formation of secondary radicals from cellular components, such as DNA, proteins or lipids. In turn, these intermediates can disturb cellular functions, such as mitochondrial respiration and more mitochondrial superoxide radicals are released (Fig. 4) (Dong and Vennerstrom 2003).

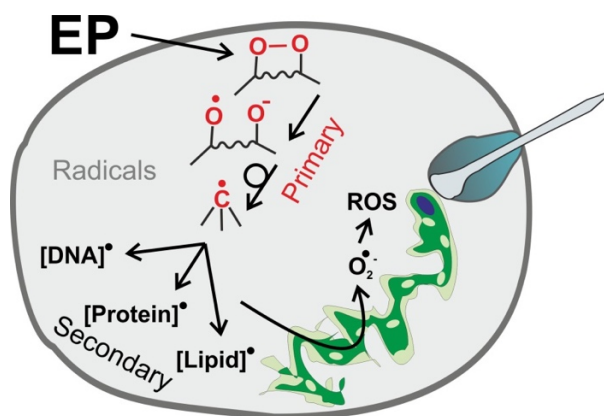


Fig. 4: Formation of primary and secondary radicals upon EP activation. After the heterolytic cleavage of the O–O bridge an oxygen-centered radical (O^{\bullet}) and an oxo anion (O^-) occur. These primary radicals are unstable and, therefore, rearrange to carbon-centered radicals (C^{\bullet}) with peroxy products. Both interact with cellular components and secondary radicals occur. The intermediates can disturb cellular functions, for example mitochondrial respiration which leads to superoxide radical ($O_2^{\bullet-}$) release and subsequently to the formation of other ROS.

Lipids, which are essential components of many cellular membranes, are primary targets of drug-derived radicals. The chain reaction of lipids with molecular oxygen is called lipid peroxidation. During this multistep reaction many free radicals, which attack the lipids in the cell membranes, are formed. The first step is the formation of a lipid radical (L^{\bullet}). This process can be induced by drug-derived radicals. The next step is the addition of molecular oxygen to

the carbon-centered lipid radical and a peroxy radical (LOO^\bullet) is generated. All primary and secondary radicals are unstable and, therefore, difficult to detect during EP actions (Yin et al. 2011).

1.9. Electron paramagnetic resonance (EPR) spectroscopy

Every molecule or atom has its own characteristic energy state. Spectroscopy measures and interprets the energy differences between atomic or molecular energy states. Depending on the molecular or atomic properties different types of electromagnetic radiation are absorbed, for example, conjugated double bonds absorbed UV-vis radiation, molecular vibrations absorbed infrared radiation or unpaired electron spins absorbed radiation in the gigahertz range. These absorptions can reveal identity, structure and dynamics of a molecule. The absorption causes a transition from the lower energy state to the higher energy state. The used frequencies vary from megahertz range through visible light to ultraviolet light. For EPR experiments a radiation in the gigahertz range, similar to a microwave oven is utilized (Weber 2011).

Energy differences in paramagnetic molecules occur because of the unpaired electrons in the sample interact with a magnetic field produced by an external magnet. Each electron has its own magnetic moment and if it is placed in a magnetic field it will adopt the state of the lowest energy when the moment of the electron is aligned with the magnetic field (parallel state $-\frac{1}{2}$) and the state of the highest energy when it is oriented against the magnetic field (antiparallel state $+\frac{1}{2}$). Furthermore, there are two important consequences for spectroscopy. On the one hand, without a magnetic field no energy differences can be measured and on the other hand, the measured energy difference depends linearly on the magnetic field, as shown in Fig. 5 (Weber 2011).

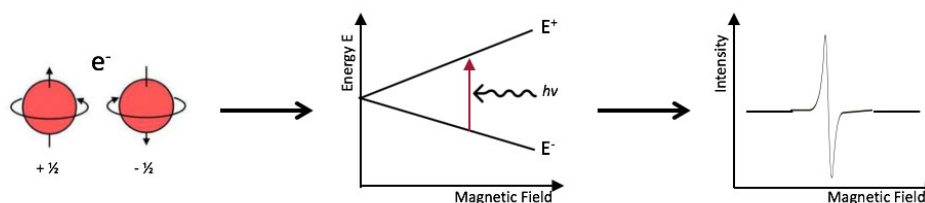


Fig. 5: Principle of EPR spectroscopy. Unpaired electrons, that are placed in a magnetic field can have a low energy state ($-\frac{1}{2}$) or a high energy state ($+\frac{1}{2}$). According to the applied magnetic field as a result in the EPR spectrum a single absorption line is detected, which is the first derivation of the absorption.

There are two strategies for measurement. First a constant magnetic field can be applied and the frequency of the electromagnetic radiation can be scanned, like in the conventional spectroscopy. Fig. 5 shows the second strategy where the electromagnetic radiation frequency is kept constant and the magnetic field is scanned. Energy differences between the two spin states of the unpaired electron depend on the magnetic field strength. When the two spin states are at a point where their energy differences match the energy of radiation applied, a peak in the absorbance will occur. For technical reasons, not the absorption directly, but the first derivative of the absorption is detected. Each unpaired electron, which gives rise to an EPR spectrum, is sensitive to its local surrounding. In each atom of a molecule or complex the nucleus produces a local magnetic field. The interaction between the nucleus and the electron is called hyperfine interaction. This interaction provides a variety of information about a molecule, like identity and number of atoms which make up a radical or complex and also the distances from the unpaired electron to the adjacent nuclei. An unpaired electron gives rise to a single EPR absorption line. Nearby nuclei with a nuclear spin > 0 split the single absorption line into multiple lines. For example, a hydrogen nucleus with nuclear spin of $\frac{1}{2}$ splits the single EPR line of the unpaired electron into two lines and a nitrogen with nuclear spin 1 into three lines. If there are two nuclear spin $\frac{1}{2}$ nuclei with the same hyperfine interaction, each of the two lines do split again into two lines and because of the same interaction two of the EPR signals will overlap. As a result, a triplet of peaks with an intensity distribution of 1:2:1 occurs (Weber 2011).

1.10. Spin trapping

Spin trapping was developed for the detection of reactive radicals in chemical systems. A spin trap, mostly a nitron or nitroso compound, is added to the target system at a high concentration. Then the spin trap reacts with any reactive short-lived radical (Fig. 6) and gives rise to a longer-lived radical adduct that accumulates and, therefore, can be detected by EPR spectroscopy. If the adduct is stable and continuous generation of the initial radical occurs, even low rates of radical formation can be detected. Depending on the stability of the spin adduct, more or less radical formation can be detected. Thus, it is important to choose the right trapping agent for each experiment. Spin trapping is used to analyze radicals from low-molecular mass compounds, like superoxide and hydroxyl radicals but also radical formation of proteins, lipids, DNA/RNA and polysaccharides in chemical and biological systems can be detected. This method has many advantages for the investigation of radicals, but also a few limitations. For example, EPR spectra of spin adducts often only

show couplings from nuclei of the spin trap but not of nuclei from the attached radical. Therefore, identification of the initial radical species is often only possible by the indirect effects of the attached radical on the nuclei of the spin trap (Hawkins and Davies 2014, Davies 2016).

1.11. Spin traps

The most widely used spin traps are nitron spin traps, such as 5,5-dimethyl-1-pyrroline N-oxide (DMPO) (Fig. 6). These traps form long-lived adducts with a wide range of radicals, for example, carbon-, oxygen- and nitrogen-centered species. The second group are the nitroso spin traps like 2-methyl-2-nitrosopropane (MNP) (Fig. 6). There the reactive radical attaches directly to nitrogen atom in the nitroso group and is, therefore, present close to the unpaired electron on the nitroxide function and provides more coupling information from the attached radical (Hawkins and Davies 2014).

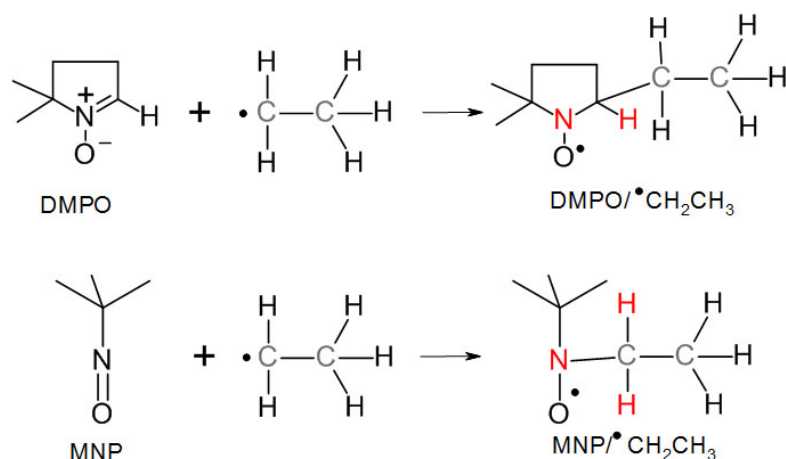


Fig. 6: Typical reactions of 5,5-dimethyl-1-pyrroline N-oxide (DMPO) and 2-methyl-2-nitrosopropane (MNP) with radicals. The reaction of DMPO or MNP with ethyl radicals forms the corresponding spin adducts (DMPO/•CH₂CH₃ or MNP/•CH₂CH₃). The atoms, which have a nuclear spin > 0 and couple with the free electron are shown in red.

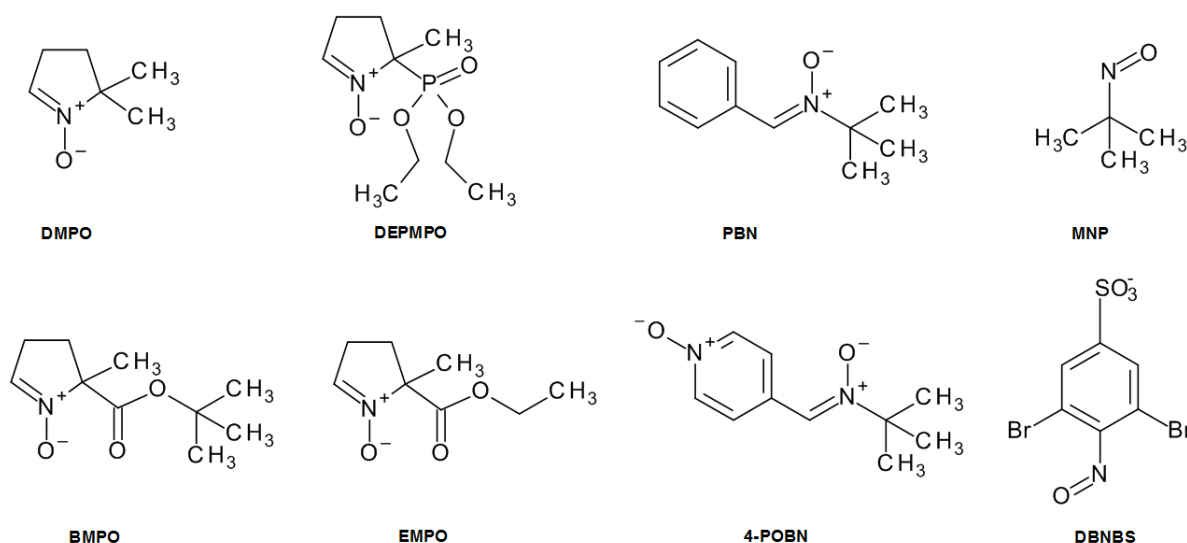


Fig. 7: Structure of commonly used spin traps. (DMPO = 5,5-dimethyl-1-pyrroline N-oxide, DEPMPO = 5-diethoxyphosphoryl-5-methyl-1-pyrroline N-oxide, PBN = α -phenyl-N-tert-butyl nitron, MNP = 2-methyl-2-nitrosopropane, BMPO = 5-tert-butoxycarbonyl 5-methyl-1-pyrroline N-oxide, EMPO = 5-(ethoxycarbonyl)-5-methyl-1-pyrroline N-oxide, POBN = α -(4-pyridyl-1-oxide)-N-tert-butyl nitron, DBNBS = 3,5-dibromo-4-nitrosobenzene sulfonic acid).

Tab. 5: Bioavailability parameters of spin traps generated with the software BIOVIA Draw (MW = molecular weight, ALogP = Partition coefficient, HAccept = hydrogen acceptors, HDonor = hydrogen donors, RotBonds = rotatable bonds, PSA = polar surface area, WS = water solubility).

Substance	Type	Rule of 5 Violations	MW	ALogP	HAccept	HDonor	RotBonds	PSA	WS
DMPO	Nitron	0	113.16	0.47	1	0	0	28.75	19
DEPMPO	Nitron	0	235.22	1.22	4	0	5	74.09	64
BMPO	Nitron	0	199.24	0.78	3	0	3	55.05	45
EMPO	Nitron	0	171.19	0.29	3	0	3	55.05	45
PBN	Nitron	0	177.24	2.97	1	0	1	28.75	19
4-POBN	Nitron	0	194.23	0.59	2	0	1	54.21	44
MNP	Nitroso	0	87.12	0.40	2	0	1	29.43	19
DBNBS	Nitroso	0	343.95	2.63	5	0	0	95.01	85

The structures of commonly used spin traps are listed in Fig. 7. To estimate their uptake into cells we calculated bioavailability parameters of spin traps using the software BIOVIA Draw, shown in Tab. 5. These parameters usually give information on how well a drug would be orally absorbed. Drugs with a good bioavailability upon oral administration are expected to adhere to “Lipinski’s Rule of Five”, e. g. meet at least four of the following criteria: less or equal to five hydrogen bond donors (the total number of nitrogen–hydrogen and oxygen–

hydrogen bonds), less or equal to ten hydrogen bond acceptors (all nitrogen or oxygen atoms), M less than 500 g/mol, an octanol-water partition coefficient ($\log P_{OW}$) less or equal to five. A high number of rotatable bond count has a negative effect on the permeation rate of drugs. On the other hand, a smaller polar surface area correlates with increased permeation rate and gives an even better indicator than the lipophilicity ($C \log P$). In addition, a sufficient water solubility is another key to good oral drug bioavailability and permeation into cells (Veber et al. 2002, Savjani et al. 2012). All spin traps (Fig. 7) adhere to these rules and should, therefore, also be taken up by cells. However, already significant differences of the $\log P_{OW}$ for the spin traps suggest differences in their rate of uptake and possibly intracellular distribution (Lipinski et al. 2001).

1.12. Problems for spin traps in cells

The lowest concentration of free radicals in an aqueous solution which can be detected is about 10^{-8} M and because of hyperfine interaction the practical limit in many cases is about 10^{-6} M (Bolton et al. 1972, Borg 1976).

Stable radicals, such as spin adducts, which accumulate to measurable concentrations and unstable radicals, which reach a high steady-state concentration by continuous generation can be detected by EPR. Many free radicals in biological systems, for example, the hydroxyl radical, are highly reactive with respect to most organic molecules. Therefore, these radicals are too short-lived for direct detection by EPR and require the use of spin traps which prolong their lifetime as spin adduct for several magnitudes of order (Dorfman and Adams 1973).

Spin trapping in biological systems has additional complications. For instance, initial drug-derived radicals can interact with certain compounds of the biological system and form secondary radicals, which superimpose EPR signals from primary radicals. Furthermore, in cellular systems upon prolonged oxidative stress primary radicals will interact with unsaturated fatty acids in membranes and thereby initiating lipid peroxidation resulting in the formation of additional radicals. These lipid radicals react with molecular oxygen forming lipid peroxy radicals. Therefore, the choice of the spin trap, its concentration, the cell number, the time point of measurement, the instrument settings and even the sample container will influence the obtained EPR spectrum (Ellington et al. 2019).

For studies in cell suspensions with spin trapping, the toxicity of the spin trap can be a problem, because in order to be able to identify free radicals, a high concentration of the spin

trap is needed. A study demonstrates that for example MNP is toxic for cultured fetal mouse liver cells when it is incubated with these cells in a concentration of 5.0 mM for 5 min (Ellington et al. 2019).

Another important point is that the spin trap, which is used to study free radical production, does not interfere with the normal activity of the enzyme, which is responsible for the radical production. For example, a study shows that PBN inhibits the neutrophil activation if its concentration is higher than 10 mM (Ellington et al. 2019).

For searching radical adducts in biological systems, it is important to know that the majority of spin adducts could be reduced to hydroxylamines, which are not detectable with EPR. This reduction of the nitroxide spin adducts is very fast and can take place even before collecting the samples. The main pathway of reduction is enzymatic, but in biological systems with low enzymatic activity a high concentration of ascorbate can dominate the reduction progress. To overcome this complications reoxidation of the reduced radical adducts can be attempted. Hence the hydroxylamine gets re-oxidized back to the nitroxide. For example, bubbling with oxygen or the addition of mild oxidant potassium ferricyanide (FeCN) are procedures for oxidation. After reoxidation the EPR spectra can be stable for several hours. One limitation of this process is that it can initiate or catalyze free radical chemical reactions *ex vivo*, which could lead to artifacts in the presence of spin traps. Thus, more studies with different oxidizing agents are necessary (Sentjurc and Mason 1992).

Therefore, spin trapping experiments in biological systems require extensive experimental optimization.

1.13. Primary radicals of endoperoxides

Tab. 6 shows for which EP primary radicals in chemical and biological systems were detected so far in three different studies. Especially in biological systems only for three EPs primary radicals can be detected although other experiments, such as the inhibition of the cytotoxic action of EPs by antioxidants, clearly indicate the involvement of radicals in EP actions. Therefore, additional studies are required to optimize spin trapping conditions for detection of EP intermediates.

Tab. 6: EPR signals detected for endoperoxides in chemical (Fe²⁺) and biological (LtP) systems. Compound abbreviations are summarized in the abbreviation list. Modified after (Geroldinger et al. 2017, 2018, Piontek 2019).

Endoperoxide	EPR signal with Fe²⁺	EPR signal with LtP
Asc	signal detected	signal detected
Art	signal detected	no signal
AcEP1117	no signal	no signal
AcEP1118	signal detected	signal detected
AcEP1129	signal detected	signal detected
AcEP1130	no signal	no signal
1062MeAcEP	no signal	no signal
DPAcEP	no signal	no signal
MB359EP	no signal	no signal
MonoGluAcEP	signal detected	no signal
mPyAcEP	no signal	no signal
mPyBuAcEP	no signal	no signal
oOMeAcEP	no signal	no signal
oPy2C8AcEP	signal detected	no signal
oPyAcEP	signal detected	no signal
DHA	no signal	no signal
Arsu	no signal	no signal

EPR spectra of the primary radicals (Tab. 6) in chemical systems (with Fe²⁺) were obtained after the reaction of 200/500 μM FeSO₄ with 500 μM EP in the presence of 40 mM DMPO or 10 mM MNP. The reactions were performed in H₂O at 25 °C. In biological systems the EPR spectra were obtained after the reaction of 2 * 10⁹ LtP/mL with 500 μM EP in the presence of 40 mM DMPO. The reaction was performed in PBS with 15 mM glucose at 26 °C (Geroldinger et al. 2017, 2018, Piontek 2019).

1.14. Aims of the current project

Previous results have shown that the detection of primary spin adducts of EPs still needs a lot of improvements to enable detection of EPR signals for a larger number of EPs. The aim of this project, therefore, is to identify the factors which influence the detection and stability of spin adduct EPR signals. The identification of these factors will focus 1) on the side of EPR

spectroscopy, 2) on the side of the spin trap and 3) on the side of the EP, in the chemical as well as in the biological system. Moreover, the exploration of the possibility to detect secondary radicals during oxidative stress in *Leishmania* triggered by EPs will be an additional point.

2. Materials and methods

2.1. Chemicals

Chemicals that were used for sample preparation and maintenance work during this study are listed in Tab. 7.

Tab. 7: List of chemicals and suppliers used for this study

Chemical	Supplier
ACN	Merck (Darmstadt, Germany)
Activated charcoal	Merck (Darmstadt, Germany)
Artemisinin (Art)	Alfa Aesa (Ward Hill, Massachusetts, USA)
Ascaridole (Asc)	self-synthesized (Monzote et al. 2009)
Brain Heart Infusion medium (BHI)	Sigma-Aldrich (St. Louis, Missouri, USA)
Chloroform	Merck (Darmstadt, Germany)
Dichloromethane	Roth (Karlsruhe, Germany)
5,5-dimethyl-1-pyrroline N-oxide (DMPO)	Sigma-Aldrich (St. Louis, Missouri, USA)
Dimethyl sulfoxide (DMSO)	VWR (Radnor, Pennsylvania, USA)
Diethylenetriaminepentaacetic acid (DTPA)	Merck (Darmstadt, Germany)
Ethyl acetate	Roth (Karlsruhe, Germany)
FeSO ₄	Merck (Darmstadt, Germany)
Glucose-Monohydrate	Merck (Darmstadt, Germany)
H ₂ O ₂	Merck (Darmstadt, Germany)
Hemin (porcine, 51280)	Sigma-Aldrich (St. Louis, Missouri, USA)
KCl	Merck (Darmstadt, Germany)
KH ₂ PO ₄	Merck (Darmstadt, Germany)
K ₂ HPO ₄	Merck (Darmstadt, Germany)
Linolenic acid	Sigma-Aldrich (St. Louis, Missouri, USA)
Methanol	Merck (Darmstadt, Germany)
MgSO ₄	VWR (Radnor, Pennsylvania, USA)
Miltefosine	Acros Organics (New Jersey, USA)
Na ₂ HPO ₄	Merck (Darmstadt, Germany)
NaCl	Merck (Darmstadt, Germany)
N-tert-butyl- α -phenylnitrone (PBN)	Sigma-Aldrich (St. Louis, Missouri, USA)
Penicillin-streptomycin solution	VWR (Radnor, Pennsylvania, USA)

Pentamidine (Pen)	Sigma-Aldrich (St. Louis, Missouri, USA)
α -(4-Pyridyl N-oxide)-N-tert-butylNitron (POBN)	Sigma-Aldrich (St. Louis, Missouri, USA)
Resazurin	Sigma-Aldrich (St. Louis, Missouri, USA)
Yeast extract (YE)	Amresco (Solon, Ohio, USA)

2.2. Cell culture of *Leishmania*

Leishmania tarentolae promastigotes (LtP) strain P10 from Jena Bioscience (Germany) were used for experiments in the biological system in this work. LtP were cultivated in brain heart infusion (BHI) medium (37 g/L, pH 7.4) in sterile ventilated 50 mL TubeSpin bioreactors (VWR) and supplemented with 5 mg/L hemin and 25.000 U/L penicillin – 25 mg/L streptomycin to avoid bacterial contamination. The parasites were grown at 26.5 °C during agitation on a shaker (0.05 s⁻¹) in an incubator (Cytoperm, Heraeus Instruments, Hanau, Germany). The culture was passaged three times a week and for experiments LtP were used one day after passage in the logarithmic growth phase. The new cell culture, after each passage, had a cell density of 18 * 10⁶ LtP/mL or 36 * 10⁶ LtP/mL, which was calculated by measuring the optical density (OD) of an 1:8 diluted aliquot at 600 nm with a U-1100 photometer (Hitachi Ltd, Tokyo, Japan). The following formula was applied for calculation (Fritsche 2008):

$$10^6 \text{ cells/mL} = \text{OD}_{600} * 0.969 * 124$$

0.969 ... conversion factor [g/L] dry weight

124 ... 1 g dry weight/L correspond to 0.124 * 10⁹ cells/mL

2.3. Viability assays

Viability assays of LtP were performed to study the effectiveness of antileishmanial compounds and potential interference of analytical reagents, such as spin traps, in viability. All viability assays of this work were carried out *in vitro* in LtP. If a substance impaired LtP viability sufficiently, the concentration of this compound, which kills 50 % of LtP (IC₅₀) was determined. Moreover, all assays were performed with 2 * 10⁶ LtP/mL over an incubation time of 48 h at 26.5 °C.

2.3.1. Viability assays with single compounds

For each assay a medium of YEM (20.7 g/L yeast extract powder, 1.2 g/L K_2HPO_4 , 0.2 g/L KH_2PO_4 , 2.9 g/L glucose, pH 7.4) and PBS (136 mM NaCl, 1.15 mM KH_2PO_4 , 14 mM Na_2HPO_4 , 2.7 mM KCl, pH 7.4) 1:1 (v/v) including 2×10^6 LtP/mL, 25.000 U/L penicillin, 25 mg/L streptomycin and 5 mg/L hemin, was prepared. In each well of rows B–H of a 96-well non-treated cell culture plate 200 μ L of this mixture were added. In row H 50 μ L of the same mixture were additionally filled for the serial dilution step. In row A only YEM/PBS was added, because this row acted as negative control (no metabolic activity, 0 % viability) and, therefore, without LtP. In row B YEM/PBS with LtP was present and represented the positive control (full metabolic activity, 100 % viability) because no substances were added. The compound stocks were added at different initial concentrations depending on the substances in row H and then five 1:5 serial dilutions were conducted, starting from row H to row C disposing the final transfer volume. On each plate four substances were tested in triplicates. The plates were incubated at 26.5 °C for 48 h. Then, 50 μ L of resazurin stock solution (in PBS) were added to each well giving a final concentration of 20 μ M. After 4 h incubation at 26.5 °C the fluorescence was measured at 590 nm emission with 560 nm excitation using a plate reader (Perkin Elmer Enspire, Germany). From these data, the viability of LtP in the absence and presence of the added compound concentrations was calculated. From plots of the viability vs. compound concentrations IC_{50} values were calculated using a four parameter logistic model (Müllebnner et al. 2010).

2.3.2. Combined viability assays with compounds and inhibitors

Combined viability assays study the possibility whether the antileishmanial effect of a compound is impaired by another compound (inhibitor). Combined viability assays were performed in a similar way as the previously described assays with the following modifications. Columns 1–6 (rows C–H) were filled with YEM/PBS containing LtP and columns 7–12 (rows C–H) with the same mixture containing in addition an inhibitor (DMPO 40 mM). In analogy the required extra volume in row H was added from these two mixtures. Then two substances in triplicates were added on both parts of the plate. The following steps, such as serial dilution, incubation, resazurin addition and measurement were performed the same way as described above. For each of the plates two compounds were tested in the presence and absence of the inhibitor. After calculation of the viability for each

well and IC_{50} values for each compound triplicate, the IC_{50} values for compound plus/minus inhibitor were compared.

2.4. EPR spectroscopy

2.4.1. Spin trapping in the biomimetic system

For detection of primary radicals in the biomimetic system the spin trap DMPO was used. Experiments in H_2O or PBS as solvent were performed. H_2O_2 , Asc or Art were reacted with $FeSO_4$ in the presence of DMPO at 25 °C. The aim of these experiments was to detect the corresponding spin adducts (DMPO/ $\cdot OH$ or DMPO/ $\cdot C$) arising from the cleavage of the peroxides H_2O_2 , Asc or Art. For the experiments with H_2O_2 , samples in 200 μL H_2O or PBS containing 40 mM DMPO, 500 μM H_2O_2 and different concentrations of $FeSO_4$ (1:1, 2:1, 4:1, 5:1, 10:1, 20:1; c/c, from 439 μM to 24 μM) were prepared. For the EP Asc the same samples containing 500 μM Asc instead of H_2O_2 with different concentrations of $FeSO_4$ (1:4, 1:2, 1:1, 2:1, 4:1, 10:1, 20:1; c/c, from 1384 μM to 24 μM) were made. After start of the reactions by addition of $FeSO_4$, 50 μL of the sample were aspirated in a glass micropipette (BLAUBRAND intraMARK, BRAND, Wertheim, Germany), sealed and inserted into the split ring resonator (Bruker MD5) of the EPR spectrometer (Bruker Digital Upgrade EMX, Rheinstetten, Germany). The measurements were started 3 min after addition of $FeSO_4$ with the following EPR spectrometer parameters: microwave frequency 9.685 GHz; microwave power 20 mW, modulation frequency 100 kHz; modulation amplitude 1 G; time constant 0.01 s; conversion time 345 ms; center field 3449.5 G; sweep width 100 G; attenuation 70 dB; x-scans 5 and y-scans 10 (resulting in 10 spectra with 1 spectrum per min). All samples were prepared and measured in triplicates.

For the EP Art, samples in 200 μL H_2O or PBS containing 40 mM DMPO, 500 μM Art and 1000 μM $FeSO_4$ were prepared. Because of the longer reaction time and poor solubility of Art a longer timescale was taken. All samples were prepared at the same time and after an incubation time of 0 h, 4 h, 8 h, 24 h and 48 h at 25 °C one duplicate with its control samples was put in the freezer at -20 °C. For measurement, a sample was thawed at room temperature for 10 min and then aspirated in a glass micropipette, sealed and inserted into the split ring resonator of the EPR spectrometer. EPR measurements were taken with the following parameters: microwave frequency 9.686 GHz; microwave power 20 mW, modulation frequency 100 kHz; modulation amplitude 1 G; time constant 0.01 s; conversion

time 345 ms; center field 3449.5 G; sweep width 100 G; attenuation 70 dB; x-scans 10 and y-scans 1. All samples were prepared and measured in duplicates.

2.4.2. Spin trapping in the biological system (LtP)

Spin trapping of Asc in LtP was performed with the spin trap DMPO. After determination of the cell density a sample of the parasite suspension containing 4×10^9 or 8×10^9 LtP was transferred into a 15 mL Falcon tube. That tube was centrifuged (Sorvall Lynx 6000 centrifuge with a BioFlexHC Rotor and bucket inserts for 15 mL tubes) at 25 °C with $1800 \times g$ for 10 min. Then, the supernatant was discarded and the cell pellet resuspended in PBS and centrifuged again. The supernatant was removed and the cell pellet resuspended in PBS containing glucose (15 mM) so that there was a final cell density of 2×10^9 or 4×10^9 LtP/mL. Aliquots of 400 μ L LtP in PBS/Glucose were prepared in 1.5 mL Eppendorf tubes with holes for aeration with 40 mM DMPO and 600 μ M Asc. Control samples were prepared the same way, but without Asc. The tubes were incubated at 26.5 °C with constant agitation (speed: 0.3 s^{-1}). At different time points 50 μ L of the suspensions were aspirated in a glass micropipette, sealed, transferred to the split ring resonator of the EPR spectrometer and measurements were started immediately. The EPR settings for each spectrum at a certain time point were: microwave frequency 9.686 GHz; microwave power 20 mW, modulation frequency 100 kHz; modulation amplitude 1 G; time constant 0.01 s; conversion time 345 ms; center field 3449.5 G; sweep width 100 G; attenuation 70 dB; x-scans 5 and y-scans 1. All samples were prepared at least in duplicates.

For experiments with Art in LtP, the cell density was determined and a sample of the parasite suspension containing 8×10^9 LtP was transferred into a 15 mL Falcon tube. Centrifugation and concentration of the cell suspension to a final cell density of 2×10^9 LtP/mL were performed the same way as described above. Two aliquots of 2 mL LtP in PBS/Glucose were prepared with 40 mM DMPO and to one sample 750 μ M Art were added. Due to the different time points for measurement the two samples were split into 200 μ L aliquots in 1.5 mL Eppendorf tubes with holes for aeration and incubated at 26.5 °C with constant agitation (speed: 0.3 s^{-1}). After different time points (0 h, 24 h, 48 h and 72 h) samples were immersed into liquid nitrogen for 30 sec and after that stored in the freezer at -20 °C. For measurements, frozen samples were incubated at a Thermomixer R (Eppendorf, Hamburg, Germany) for 10 min at 27 °C with 800 rpm and, afterwards, aspirated in a glass micropipette and inserted into the split ring resonator of the EPR spectrometer. EPR measurements were taken with the following parameters: microwave frequency 9.686 GHz; microwave power

20 mW, modulation frequency 100 kHz; modulation amplitude 1 G; time constant 0.01 s; conversion time 345 ms; center field 3449.5 G; sweep width 100 G; attenuation 70 dB; x-scans 10 and y-scans 1. All samples were prepared and measured in duplicates.

2.4.3. Extraction and spin trapping of lipid-derived radicals

The extraction of lipid-derived spin adducts was performed in different variations. Therefore, extractions with LtP, without LtP and in model systems with linolenic acid (LA) were performed. The detailed differences or additional processes of the extractions are listed in the tables of the results part (see 3.2.3., Tab. 10–14). For extractions with LtP, the cell density was determined, and a sample of the parasite suspension containing 8×10^9 LtP was transferred into a 15 mL Falcon tube. The tube was centrifuged at 20 °C with $1800 \times g$ for 10 min. Then, the supernatant was discarded and the cell pellet was resuspended in PBS and centrifuged again. The supernatant was removed and the cell pellet resuspended in PBS containing glucose (15 mM) so that there was a final cell density of 2×10^9 LtP/mL. Aliquots of 1 mL LtP in PBS/Glucose were prepared in 1.5 mL Eppendorf tubes with holes for aeration and 40 mM DMPO was added. Additionally, 600 μ M or 1000 μ M Asc were added to one sample. For model systems containing LA, samples in 1 mL PBS with 40 mM DMPO, 5 mM LA, 100 μ M DTPA and 100 μ M FeSO₄ were prepared. Moreover, different control samples containing 1 mL PBS and 40 mM DMPO, 1 mL PBS/Glucose and 40 mM DMPO, 1 mL PBS or 1 mL PBS/Glucose were made. All samples were incubated at 26.5 °C with constant agitation (speed: 0.3 s^{-1}). At different time points samples were extracted. Therefore, a 15 mL Falcon tube with 200 μ L H₂O and 4.5 mL cold Folch reagent composed of methanol (CH₃OH) and dichloromethane (CH₂Cl₂) (1:2, v/v) were prepared. Then, 1 mL sample was added and vortexed for 5 min. After that, 250 μ L saturated NaCl were added and vortex again. For phase separation the tubes were centrifuged at 4 °C for 5 min at $5000 \times g$. The lower phase of each sample was transferred in a new 15 mL Falcon tube and evaporated in a stream of N₂ until the tube was dry. In some experiments, samples were dried with MgSO₄ before evaporation with N₂ by adding a few grains of MgSO₄ to the sample. After mixing, the samples with MgSO₄ were centrifuged at 4 °C for 5 min at $5000 \times g$ (Hettich® Universal 16R centrifuge Tuttlingen, Germany). The supernatant was transferred in a new 15 mL Falcon tube and evaporated in a stream of N₂ until the tube was dry. For EPR measurements 100 μ L of ethyl acetate (EtOAc) were added to the dry tube and vortexed for 1 min. Then, 50 μ L of the solutions were aspirated in a glass micropipette, sealed, transferred to the split ring resonator of the EPR spectrometer and measurements were started immediately with the

following EPR settings for each spectrum: microwave frequency 9.686 GHz; microwave power 20 mW, modulation frequency 100 kHz; modulation amplitude 1 G; time constant 0.01 s; conversion time 345 ms; center field 3449.5 G; sweep width 100 G; attenuation 70 dB; x-scans 5 and y-scans 1.

2.5. Simulation and data analysis

For comparison of the obtained EPR spectra from the experiments, they were simulated in the software WINSIM (Duling 1994). A curve with parameters matching the observed radicals was generated to reveal the respective coupling constants.

Graphing and calculations were carried out using Microsoft Excel (Microsoft, Washington, USA). For all experiments mean and standard deviation of the data were calculated. The number of replicates is listed at the respective figure or table of the experiment. The IC₅₀ values determined from viability assays were calculated from a non-linear concentration-response curve using a four-parameter logistic model (Müllebner et al. 2010).

3. Results

3.1. Influence of EPs on viability of LtP

The viability is the ability of a cell to survive and to be metabolically active in the presence and absence of added substances. With these methods, many substances in different concentrations can be tested for their effect against specific cells. Dose response curves for different compounds were obtained and for each compound IC_{50} values were calculated. Fig. 8 shows one example of a dose response curve for the EP Art.

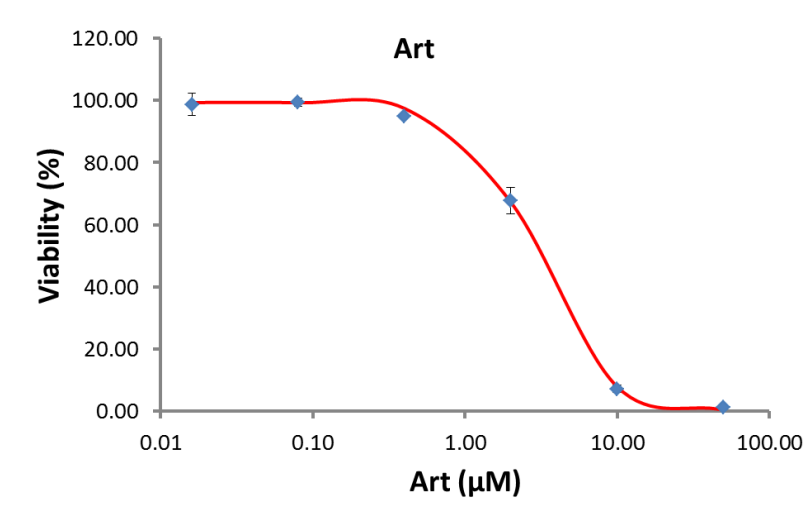


Fig. 8: Dose response curve of the viability of LtP as a function of different concentrations of Art (0.02 µM, 0.08 µM, 0.40 µM, 2.00 µM, 10.00 µM and 50.00 µM). The IC_{50} value for Art obtained from this experiment was 2.91 ± 0.10 µM. Individual data points represent mean \pm SD of triplicate measurements.

In Tab. 8 all tested substances of viability assays with single compounds and their respective IC_{50} values are listed. As expected for antileishmanial compounds (Pen, Mil, Asc, Art) low to moderate IC_{50} values in the µM range were observed. For spin traps (DMPO, PBN, POBN) high IC_{50} values were observed. This is important, because all EPR experiments in LtP were done with DMPO as spin trap.

Tab. 8: IC₅₀ values of antileishmanial compounds and spin traps. The IC₅₀ values were obtained by using resazurin viability assays of serial dilutions in 96 well plates of respective compounds with an endpoint of 48 h and starting with 2 * 10⁶ LtP/mL. The data represent mean ± SD.

Compound	IC ₅₀ (μM) mean ± SD	Viability minimum (% at highest conc.)	n
Pen	1.20 ± 0.48	-	6
Mil	0.144 ± 0.064	-	5
Asc	55.7 ± 23.2	-	5
Art	2.02 ± 0.53	-	5
DMPO	> 100000	68 ± 3	2
PBN	1471 ± 474	-	2
POBN	4677 ± 38	-	2

The results of the combined viability assays with compounds and inhibitors are shown in Tab. 9. It shows that DMPO functioned as an inhibitor, because the IC₅₀ values of the substances in the presence of DMPO are higher than in the absence of DMPO.

Tab. 9 IC₅₀ values of antileishmanial compounds in the presence or absence of the spin trap DMPO and its influence on the viability of LtP. The IC₅₀ values were obtained by using resazurin combined viability assays of serial dilutions in 96 well plates of respective compounds in the presence and absence of DMPO with an endpoint of 48 h and starting with 2 * 10⁶ LtP/mL. The data represent mean ± SD.

Compound	IC ₅₀ (μM) mean ± SD	Inhibitor	IC ₅₀ (μM) mean ± SD	Change (%)
Asc	51.6 ± 8.1	DMPO (40 mM)	131 ± 3	253
Art	2.11 ± 0.17	DMPO (40 mM)	3.50 ± 0.07	165

3.2. Detection of radicals triggered by H₂O₂ and EPs

3.2.1. Spin trapping in biomimetic systems

For the detection of spin adducts from primary radicals, we started with experiments in a biomimetic system. Thereby, we intended to observe the required conditions to obtain EPR signals and study the influence of PBS on the radical formation for following experiments in the biological system.

3.2.1.1. H₂O₂-derived radicals in water

In the first step, we studied the reaction of H₂O₂ with iron (Fe²⁺). For this purpose, we used the spin trap DMPO. The reaction took place in H₂O. The corresponding spin adduct (DMPO/•OH) was formed and detected by EPR. Fig. 9 shows the obtained spectrum. Every spectrum shown in the results part represents the first derivative of the absorption.

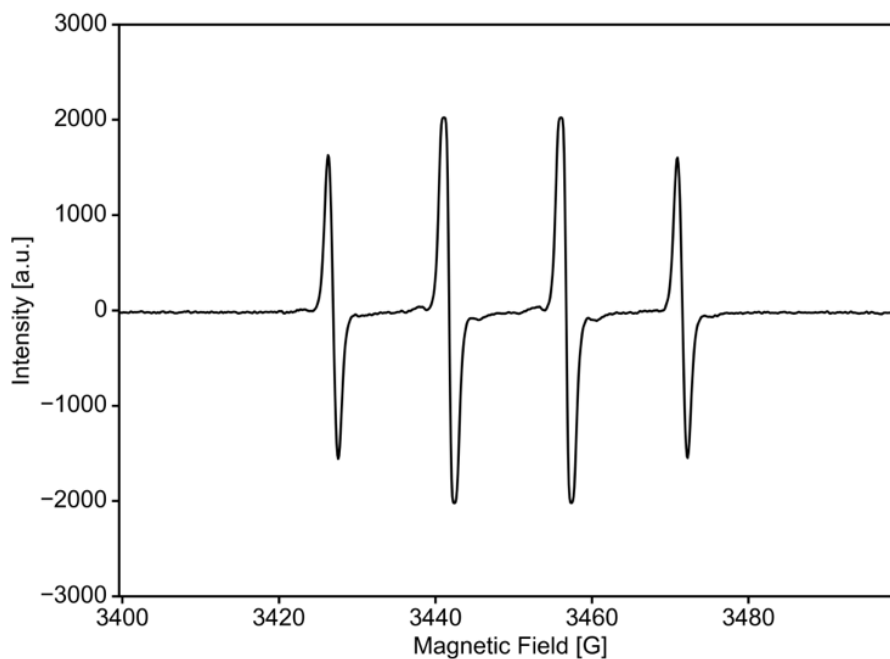


Fig. 9: EPR spectrum recorded after 3 min incubation of H₂O₂ with FeSO₄ in the presence of DMPO in H₂O at room temperature. The reaction mixture contained in 200 μ L H₂O with 42 mM DMPO, 472 μ M H₂O₂ and 94 μ M FeSO₄. The graph shows a representative spectrum of three independent experiments.

To identify the radical species in the EPR spectrum of Fig. 9 a simulation was made with the software WINSIM in order to obtain coupling constants for the detected radicals. These coupling constants reflect the interaction of the unpaired electron with adjacent nuclei, which have a nuclear spin > 0 . Fig. 10 shows the EPR spectrum of the experimental measurement in comparison to the simulation. The obtained coupling constants $a_N = 15.1$ G and $a_H = 14.5$ G are compatible with the presence of a DMPO/•OH adduct (Buettner 1987). In the simulation the DMPO/•OH adduct explained 100 % of the signal. The percentage is a measure for a relative contribution of a certain spin adduct to the whole signal.

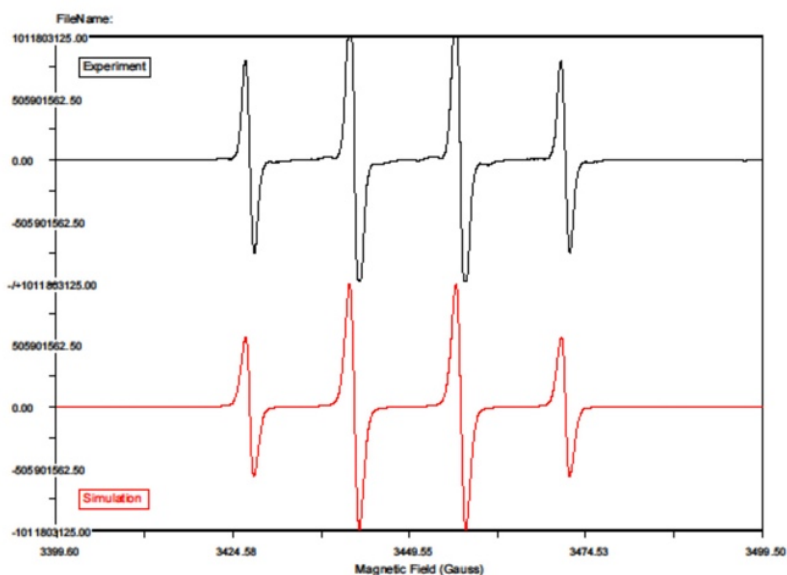


Fig. 10: EPR spectrum recorded after incubation of $472 \mu\text{M}$ H_2O_2 with $94 \mu\text{M}$ FeSO_4 in the presence of 42 mM DMPO in water and the corresponding simulated spectrum generated with the WINSIM software. The coupling constants obtained from this simulation were $a_N = 15.1 \text{ G}$ and $a_H = 14.5 \text{ G}$.

To follow the development of the DMPO/ $\cdot\text{OH}$ adduct in water with different Fe^{2+} concentrations, we measured the peak-to-peak intensity of the low-field peak (I_{pp}) over 10 min. The low-field peak represents the peak of the EPR spectrum at the lowest magnetic field. The time course of the EPR signal intensity during the reaction of H_2O_2 in the presence of DMPO dependent on the Fe^{2+} concentration is shown in Fig. 11. The time scale t_{EPR} used in this graph represents the time after start of the EPR recording. Since time is required for mixing, capillary sealing, sample transfer and tuning, t_{mixing} is usually t_{EPR} plus 3 min. The different I_{pp} -time profiles clearly show that an altered $\text{H}_2\text{O}_2:\text{Fe}^{2+}$ ratio does not only alter the maximum I_{pp} , but also its time dependence. To make this non-linear relationship visible, Fig. 12 displays the EPR intensity detected 3 min after mixing with different $\text{H}_2\text{O}_2:\text{Fe}^{2+}$ ratios.

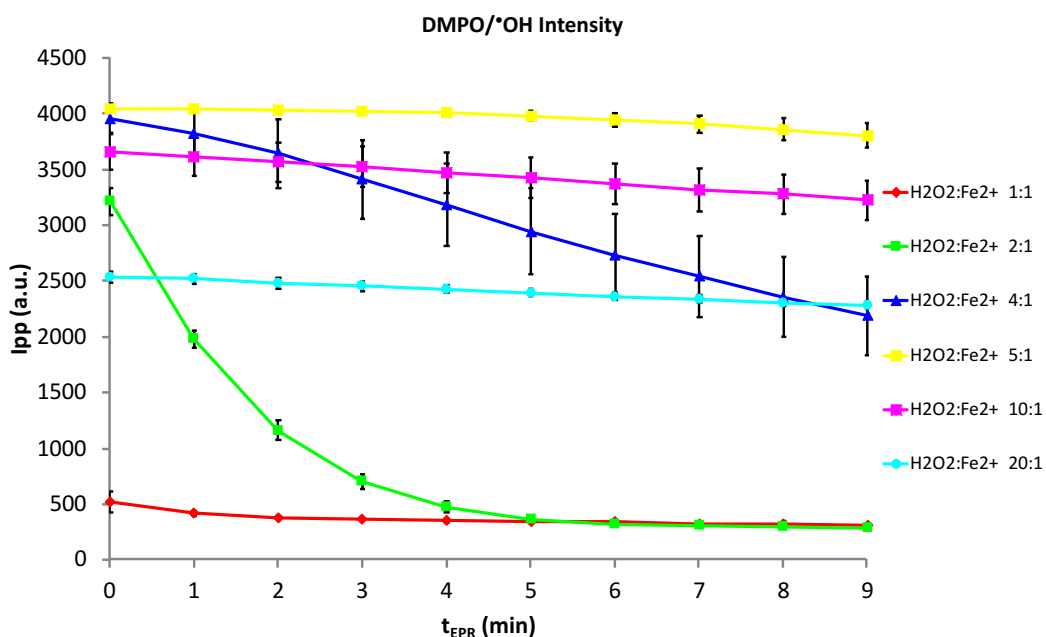


Fig. 11: Time- and concentration-dependent development of the DMPO/•OH adduct intensity (I_{pp}) in 200 μ L water with 42 mM DMPO, 472 μ M H_2O_2 and different concentrations of $FeSO_4$, resulting in $H_2O_2:Fe^{2+}$ ratios of 1:1 (472 μ M), 2:1, 4:1, 5:1, 10:1 and 20:1. The time scale represents the time after start of the measurement (t_{EPR}) and is the time since mixing minus 3 min. Data represent mean \pm SD ($n = 3$).

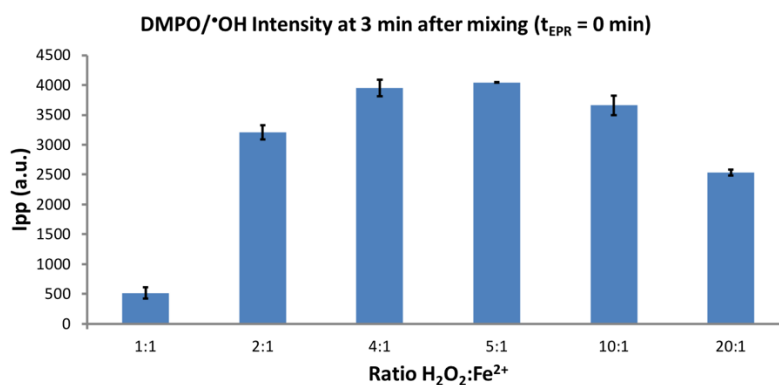


Fig. 12: Detected intensity (I_{pp}) of the DMPO/•OH adduct 3 min after mixing ($t_{EPR} = 0$) in 200 μ L water with 42 mM DMPO, 472 μ M H_2O_2 and different concentrations of $FeSO_4$, resulting in $H_2O_2:Fe^{2+}$ ratios of 1:1 (472 μ M), 2:1, 4:1, 5:1, 10:1 and 20:1. Data represent mean \pm SD ($n = 3$).

The initial I_{pp} of the DMPO/•OH adduct was highly dependent on the $H_2O_2:Fe^{2+}$ ratio. Especially the decline of I_{pp} at lower ratios appeared to be counter intuitive since in the presence of more Fe^{2+} less DMPO/•OH was detected.

To evaluate the stability of the corresponding spin adducts under our experimental conditions we calculated the intensity slope during the first two minutes ($t_{\text{EPR}} = 0, 1, 2$ min, from three spectra) in samples with different ratios of H_2O_2 and Fe^{2+} (Fig. 13).

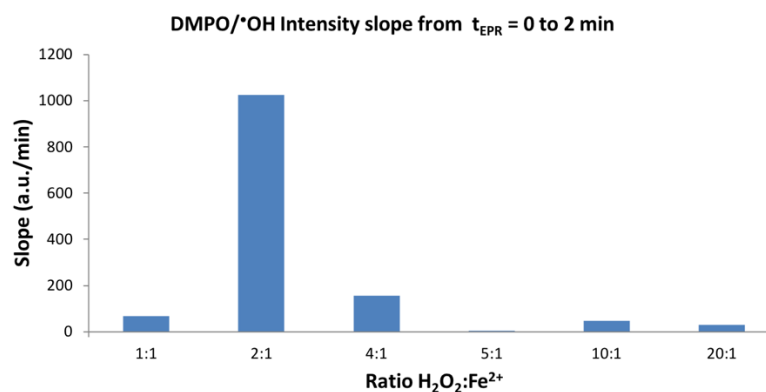


Fig. 13: Slope of the DMPO/•OH intensity over the first three minutes ($t_{\text{EPR}} = 0, 1, 2$ min). The EPR measurements were started 3 min after mixing of 200 μL water with 42 mM DMPO, 472 μM H_2O_2 and different concentrations of FeSO_4 (ratio 1:1 (472 μM), 2:1, 4:1, 5:1, 10:1 and 20:1). Data represent mean \pm SD ($n = 3$).

A high slope at the 2:1 $\text{H}_2\text{O}_2:\text{Fe}^{2+}$ ratio was observed indicating a highly unstable lpp for the spin adduct under these conditions.

3.2.1.2. H_2O_2 -derived radicals in PBS

Most experiments with EPs in the biological system of LtP are performed in PBS buffer. Therefore, it was logical to study H_2O_2 -derived radicals in PBS instead of H_2O to explore the influence of PBS on the radical formation. Again, we studied the influence of PBS on spin trapping of hydroxyl radicals over 10 min under similar conditions as in the experiments with water (Fig. 14).

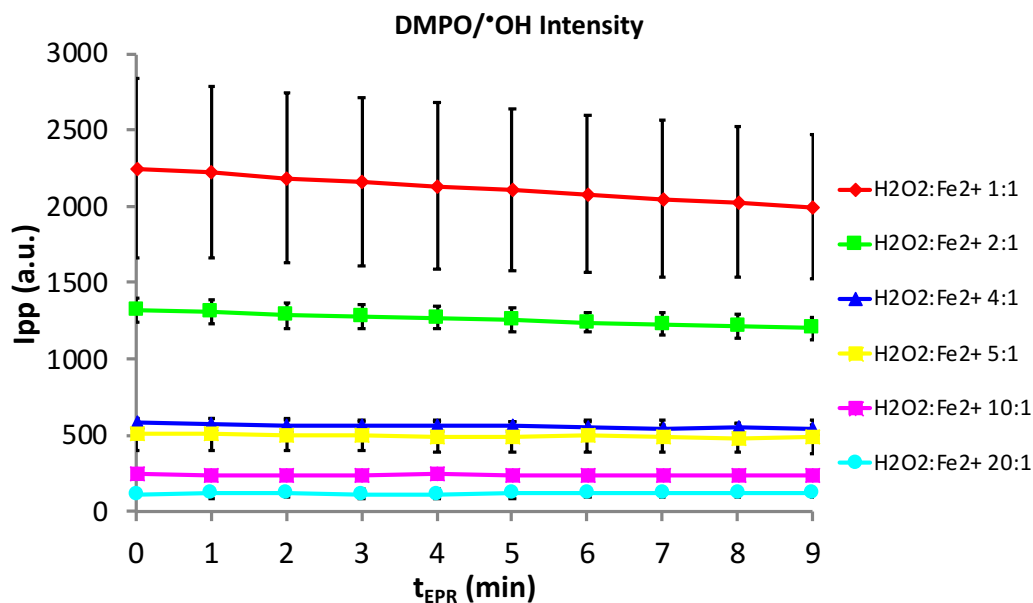


Fig. 14: Time- and concentration-dependent development of the DMPO/•OH adduct intensity (I_{pp}) in 200 μ L PBS with 39 mM DMPO, 439 μ M H₂O₂ and different concentrations of FeSO₄, resulting in H₂O₂:Fe²⁺ ratios of 1:1 (439 μ M), 2:1, 4:1, 5:1, 10:1 and 20:1. The time scale represents the time after start of the measurement (t_{EPR}) and is the time since mixing minus 3 min. Data represent mean \pm SD ($n = 3$).

In contrast to experiments in water, in PBS all DMPO/•OH signal intensities (I_{pp}) were fairly stable over time. Furthermore, consistently in PBS in the presence of increasing concentrations of Fe²⁺ increasing intensities of the DMPO/•OH adduct were observed, which is unlike the reaction in water.

3.2.1.3. Asc-derived radicals in water

The next step was to study spin trapping of EP-derived radicals. For these experiments, we chose Asc and performed similar experiments in water and PBS as described before. The experiments with Asc in water in the presence of DMPO and Fe²⁺ resulted in an EPR spectrum as shown in Fig. 15.

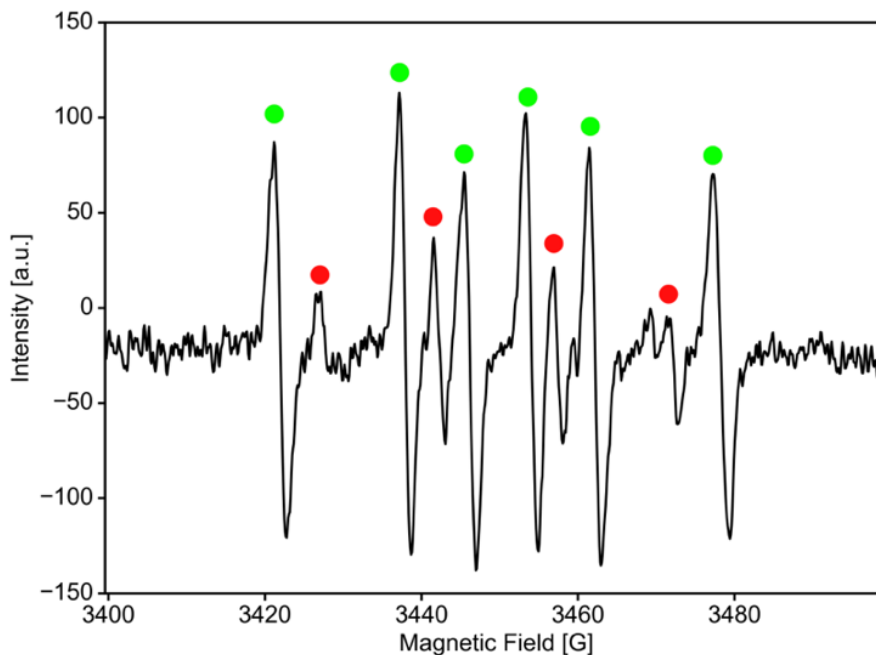


Fig. 15: EPR spectrum recorded after 3 min incubation of Asc with FeSO_4 in the presence of DMPO in water. The reaction mixture contained in 200 μL H_2O , 39 mM DMPO, 439 μM Asc and 439 μM FeSO_4 . The EPR signal is a composite spectrum of different spin adducts. Simulations (see below) revealed that EPR lines labeled with a green dot can be assigned to a DMPO/ $\cdot\text{C}$ adduct and lines labeled with a red dot to a DMPO/ $\cdot\text{OH}$ adduct. The graph shows a representative spectrum of three independent experiments.

A simulation of the EPR spectrum shown in Fig. 15 was made with the software WINSIM to obtain the coupling constants for the detected radicals. Fig. 16 shows the experimental EPR spectrum together with the simulated spectrum. The derived coupling constants are compatible with the presence of a DMPO/ $\cdot\text{OH}$ adduct (15.3 %) and a DMPO/ $\cdot\text{C}$ adduct (84.7 %).

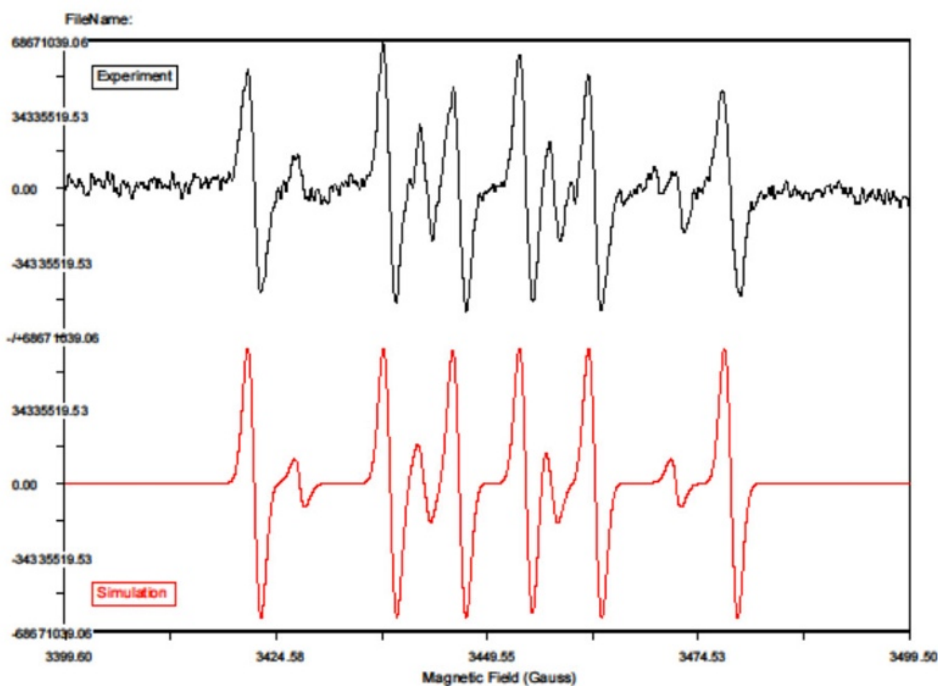


Fig. 16: EPR spectrum recorded after incubation of 439 μM Asc with 439 μM FeSO_4 in the presence of 39 mM DMPO in water and the corresponding simulated spectrum generated with the WINSIM software. The coupling constants obtained from this simulation for the high intensity component $a_N = 16.1$ G and $a_H = 24.2$ G suggest the presence of a DMPO/ $\cdot\text{C}$ adduct and for the low intensity component $a_N = 15$ G and $a_H = 14.4$ G the presence of a DMPO/ $\cdot\text{OH}$ adduct.

To follow the development of the DMPO/ $\cdot\text{C}$ and DMPO/ $\cdot\text{OH}$ adduct in water with different Fe^{2+} concentrations we measured the Ipp over 10 min. The time course of the EPR signal intensities at different Asc: Fe^{2+} ratios is shown in Fig. 17 for the DMPO/ $\cdot\text{C}$ adduct and in Fig. 18 for the DMPO/ $\cdot\text{OH}$ adduct. The influence of increasing Fe^{2+} concentrations on the DMPO/ $\cdot\text{C}$ adduct formation was clearly visible, however, for the DMPO/ $\cdot\text{OH}$ no such correlation was observed.

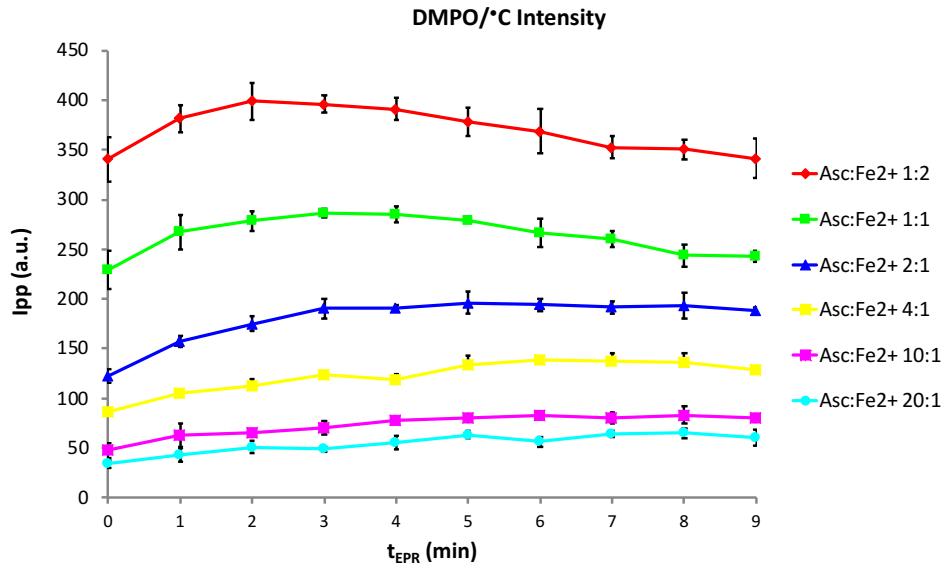


Fig. 17: Time- and concentration-dependent development of the DMPO/•C adduct intensity (Ipp) in 200 μ L water with 39 mM DMPO, 439 μ M Asc and different concentrations of FeSO₄ (Asc:Fe²⁺ ratios: 1:2 (878 μ M), 1:1, 2:1, 4:1, 10:1 and 20:1). Data represent mean \pm SD (n = 3).

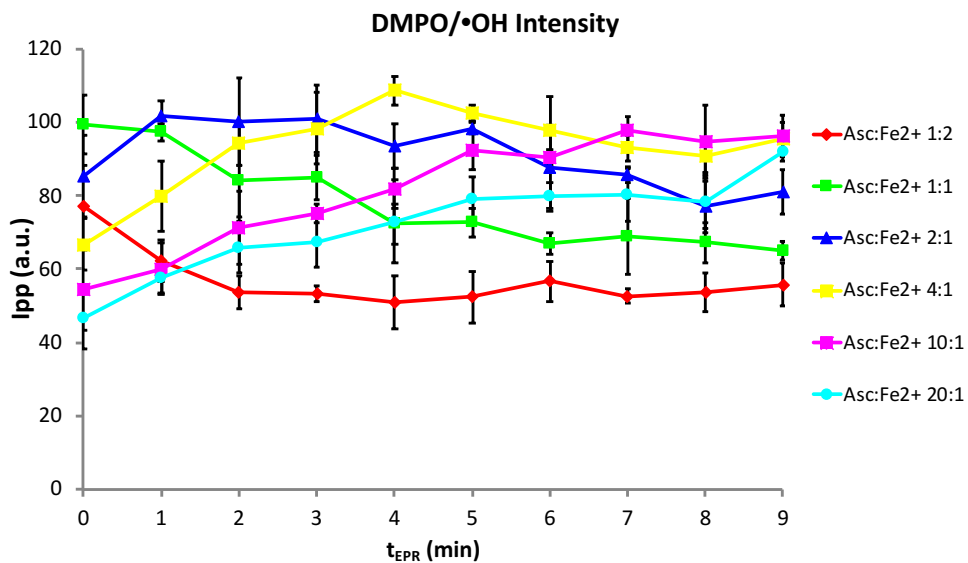


Fig. 18: Time- and concentration-dependent development of the DMPO/•OH adduct intensity (Ipp) in 200 μ L water with 39 mM DMPO, 439 μ M Asc and different concentrations of FeSO₄ (Asc:Fe²⁺ ratios: 1:2 (878 μ M), 1:1, 2:1, 4:1, 10:1 and 20:1). Data represent mean \pm SD (n = 3).

3.2.1.4. Asc-derived radicals in PBS

In analogy to the experiments in water, the reaction of Asc with Fe^{2+} in the presence of DMPO was studied in PBS, since experiments in the biological system (LtP) will use PBS as buffer. It was important to study the influence of PBS on the radical formation of the EP Asc. Fig. 19 shows an EPR spectrum observed after the reaction of Asc with Fe^{2+} in PBS. The simulation of the spectrum with the software WINSIM is displayed in Fig. 20. The coupling constants obtained by simulation are compatible with the presence of a DMPO/ $\cdot\text{C}$ adduct arising from the carbon-centered radicals. In contrast to the corresponding experiments in water, in PBS no other spin adduct was observed.

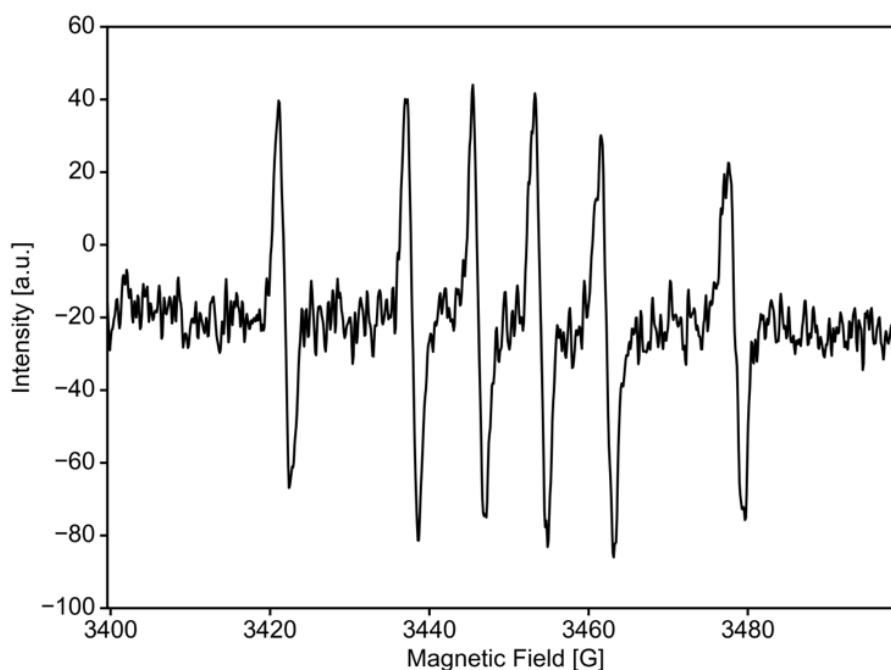


Fig. 19: EPR spectrum obtained after 3 min incubation of Asc (346 μM) with FeSO_4 (1384 μM) in 200 μL PBS in the presence of DMPO (31 mM). The graph shows a representative spectrum of three independent experiments.

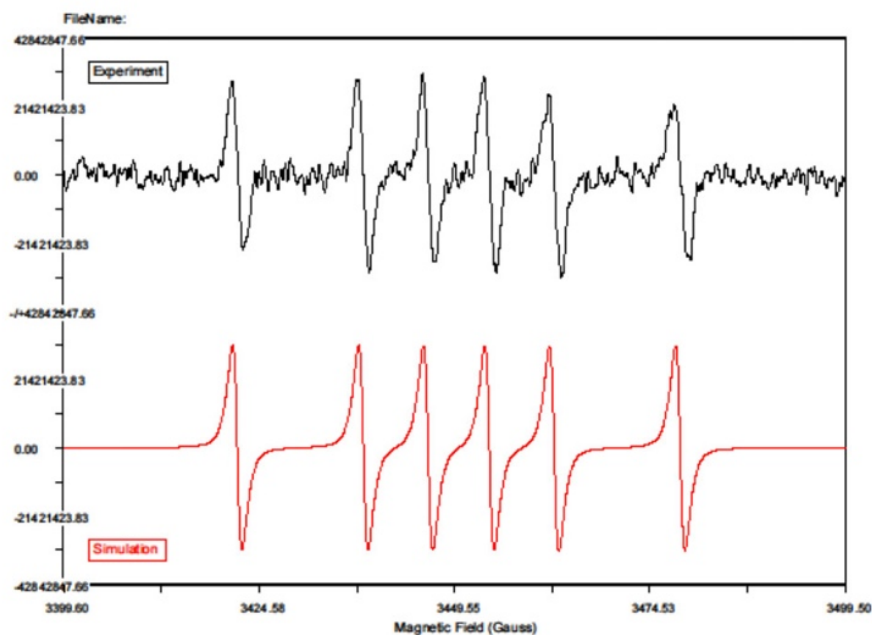


Fig. 20: EPR spectrum recorded after incubation of 346 μM Asc with 1384 μM FeSO_4 in the presence of 31 mM DMPO in PBS and the corresponding simulated spectrum generated with the WINSIM software. The coupling constants obtained from this simulation are $a_N = 16.1$ G and $a_H = 24.4$ G corresponding to a DMPO/ $\cdot\text{C}$ adduct.

To follow the time-dependent development of the DMPO/•C adduct in PBS with different Fe²⁺ concentrations we measured the I_{pp} over 10 min. The resulting time course of the EPR signal intensity of Asc in the presence of DMPO dependent on the Fe²⁺ concentration is shown in Fig. 21. Again, with increasing Fe²⁺ concentrations an increasing DMPO/•C adduct formation was observed. In contrast to experiments in water, in PBS the maximal intensity of the DMPO/•C adduct appeared later.

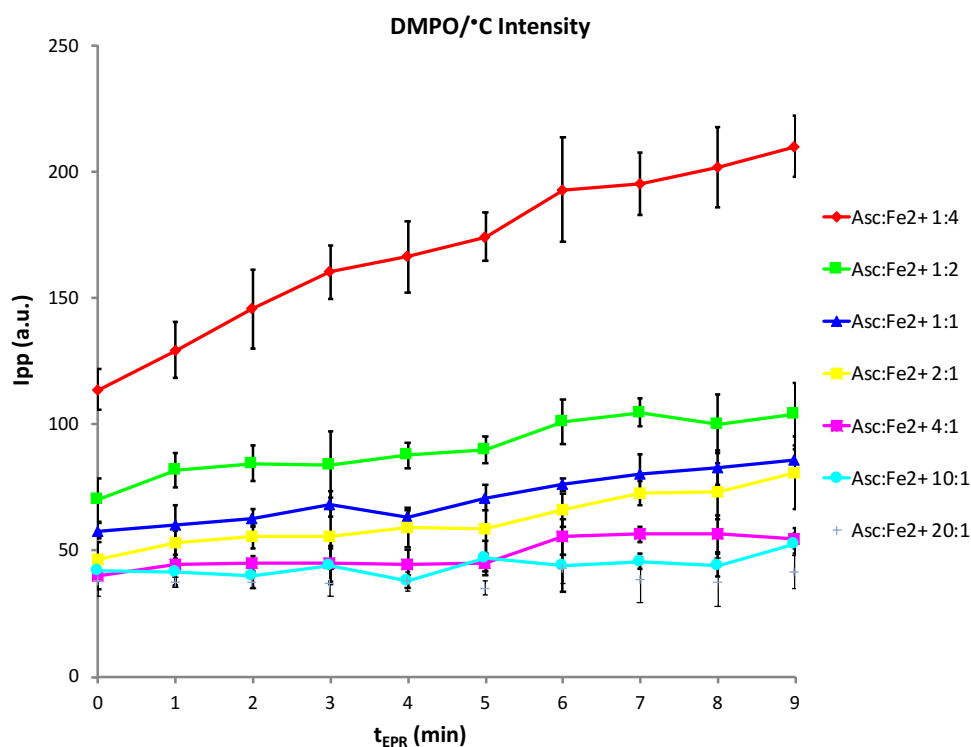


Fig. 21: Time- and concentration-dependent development of the DMPO/•C adduct intensity (I_{pp}) in 200 μL PBS upon incubation of 31 mM DMPO with 346 μM Asc and different concentrations of FeSO₄ (Asc:Fe²⁺ ratios: 1:4 (1384 μM), 1:2, 1:1, 2:1, 4:1, 10:1 and 20:1). Data represent mean ± SD (n = 3).

3.2.1.5. Art-derived radicals in water

To study spin trapping of other EP-derived radicals, we additionally made experiments with Art. The first experiments with Art were performed in water in the presence of DMPO and Fe²⁺. A resulting experimental spectrum together with its simulation made with the software WINSIM is shown in Fig. 22. The derived coupling constants can be assigned to the presence of a DMPO/•OH adduct (44.8 %) and a DMPO/•C adduct (55.3 %).

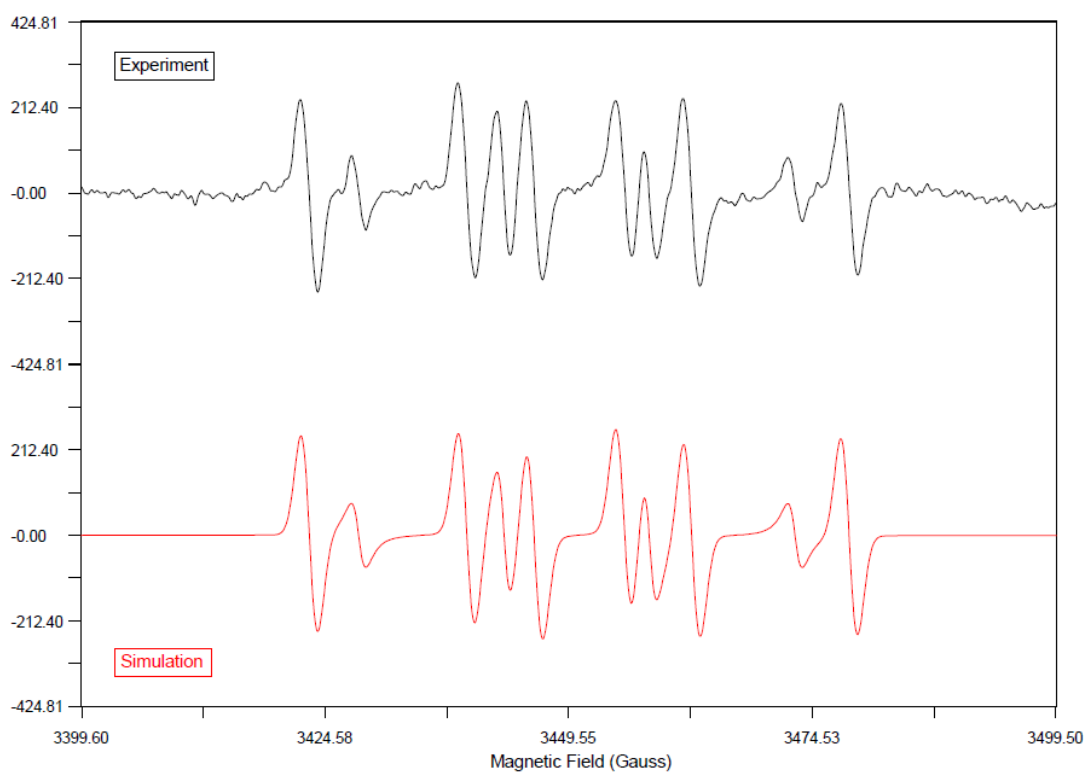


Fig. 22: EPR spectrum recorded after incubation of 497 μM Art with 1086 μM FeSO_4 in the presence of 39 mM DMPO in water and the corresponding simulated spectrum generated with the WINSIM software. The coupling constants obtained from this simulation for the high intensity component $a_N = 16.1$ G and $a_H = 23.1$ G suggest the presence of a DMPO/ $\cdot\text{C}$ adduct and for the low intensity component $a_N = 14.9$ G and $a_H = 14.9$ G the presence of a DMPO/ $\cdot\text{OH}$ adduct.

Additionally, control samples without Art were measured. A resulting experimental spectrum of the reaction of DMPO with Fe^{2+} in water and its simulation made with the software WINSIM is shown in Fig. 23. The derived coupling constants can be assigned to the presence of a DMPO/ $\cdot\text{OH}$ adduct (100 %).

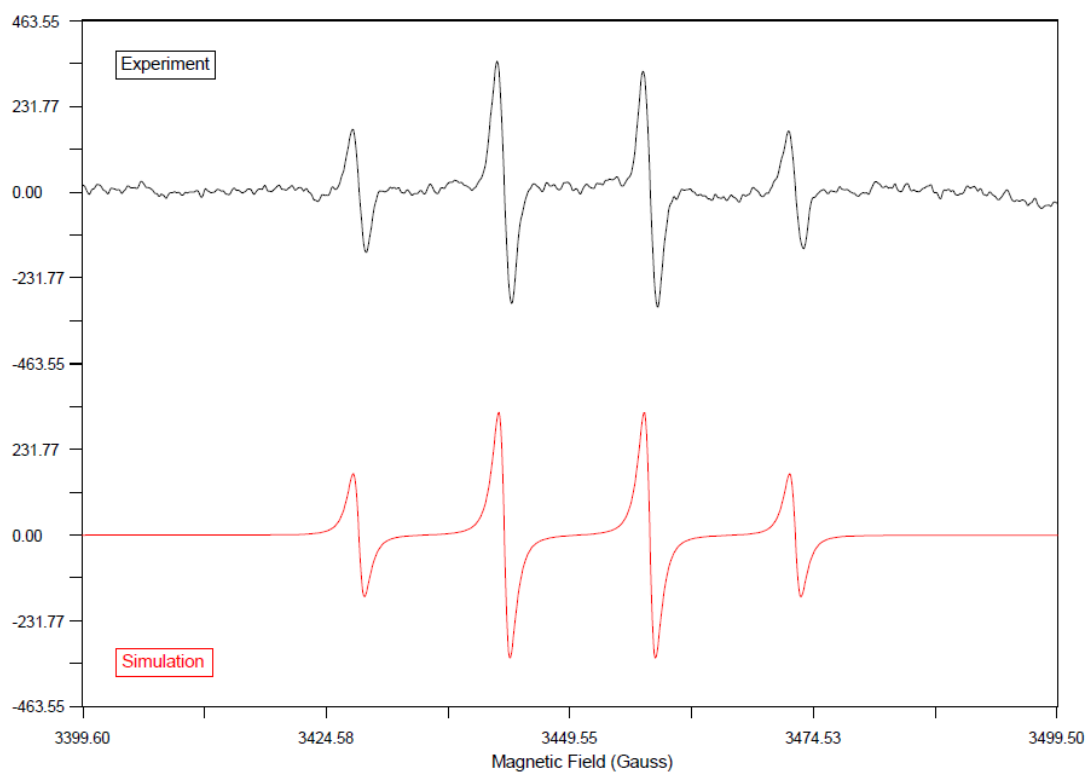


Fig. 23: EPR spectrum recorded after incubation of 1100 μM FeSO_4 with 39 mM DMPO in water and the corresponding simulated spectrum generated with the WINSIM software. The coupling constants obtained from this simulation $a_N = 14.9$ G and $a_H = 14.9$ G suggest the presence of a DMPO/ $^{\bullet}\text{OH}$ adduct.

To follow the development of the DMPO/•C and DMPO/•OH adducts in water over a long timescale, we measured the Ipp over 48 h. The time course of the EPR signal intensities for the DMPO/•C and DMPO/•OH adduct for Art in the presence of DMPO and Fe²⁺ is shown in Fig. 24. Over the first eight hours both signal intensities are stable. EPR signal intensities of the control samples without Art are shown in Fig. 25. No DMPO/•C signals were detected and the DMPO/•OH adduct intensity is stable over the measured time.

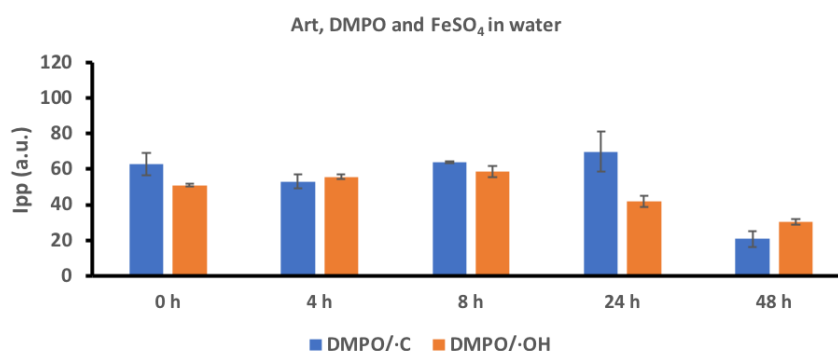


Fig. 24: Time-dependent development of the DMPO/•C and DMPO/•OH adduct intensities (Ipp) in 200 μ L water with 39 mM DMPO, 497 μ M Art and 1086 μ M FeSO₄. Samples were frozen at 0 h, 4 h, 8 h, 24 h and 48 h and measured after 10 min incubation at room temperature. Data represent mean \pm SD (n = 2).

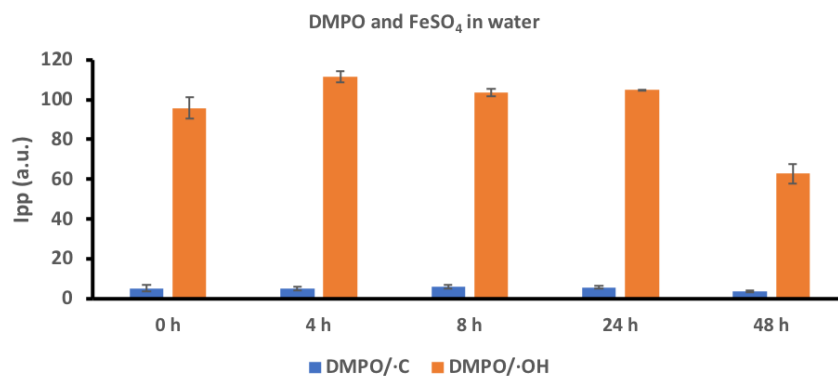


Fig. 25: Time-dependent development of the DMPO/•C and DMPO/•OH adduct intensities (Ipp) in 200 μ L water with 39 mM DMPO and 1100 μ M FeSO₄. Samples were frozen at 0 h, 4 h, 8 h, 24 h and 48 h and measured after 10 min incubation at room temperature. Data represent mean \pm SD (n = 2).

3.2.1.6. Art-derived radicals in PBS

In analogy to the experiments in water, the reaction of Art with Fe^{2+} in the presence of DMPO was studied in PBS, because the next step would be similar experiments with Art in LtP suspended in PBS. Thus, it is important to study the influence of PBS on the radical formation of Art. Similar to the experiments in water, samples are measured over 48 h and the results for samples with Art in the presence of DMPO and Fe^{2+} in PBS are shown in Fig. 26. Under these conditions, no signals for DMPO/ $\cdot\text{C}$ and DMPO/ $\cdot\text{OH}$ adducts were detected. The results for the control samples without Art are shown in Fig. 27 and also no signals were measured.

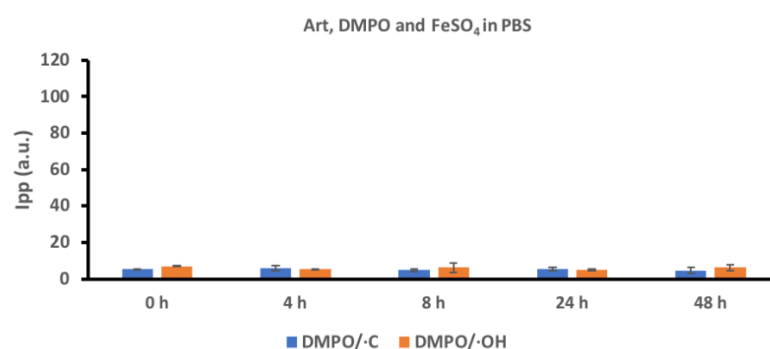


Fig. 26: Time-dependent development of the DMPO/ $\cdot\text{C}$ and DMPO/ $\cdot\text{OH}$ adduct intensities (Ipp) in 200 μL PBS with 39 mM DMPO, 497 μM Art and 1086 μM FeSO_4 . Samples were frozen at 0 h, 4 h, 8 h, 24 h and 48 h and measured after 10 min incubation at room temperature. Data represent mean \pm SD (n = 2).

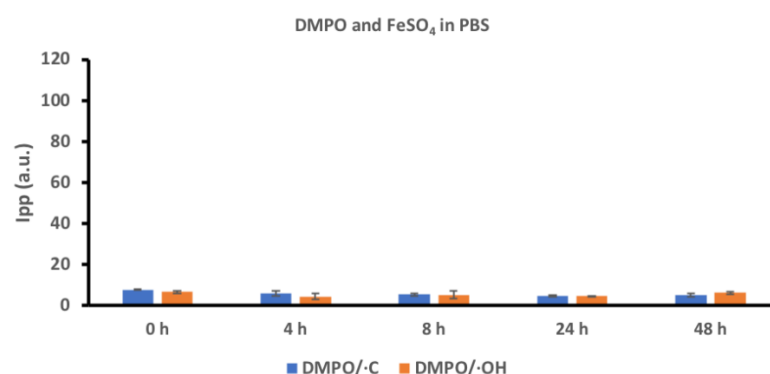


Fig. 27: Time-dependent development of the DMPO/ $\cdot\text{C}$ and DMPO/ $\cdot\text{OH}$ adduct intensities (Ipp) in 200 μL PBS with 39 mM DMPO and 1100 μM FeSO_4 . Samples were frozen at 0 h, 4 h, 8 h, 24 h and 48 h and measured after 10 min incubation at room temperature. Data represent mean \pm SD (n = 2).

3.2.2. Spin trapping of EP-derived radicals in LtP

After spin trapping experiments with different EPs in biomimetic systems, analogous experiments in LtP, our biological system were performed. Therefore, Asc and Art were tested with different cell numbers and concentrations.

3.2.2.1. Asc-derived radicals in LtP

To study EP-derived radicals in LtP, as a first step experiments with Asc were performed. The reaction of Asc with 2×10^9 or 4×10^9 LtP/mL in the presence of DMPO in PBS/Glucose (15 mM) was observed. A resulting experimental spectrum together with its simulation made with the software WINSIM is shown in Fig. 28 for a cell number of 2×10^9 LtP/mL and in Fig. 29 for a cell number of 4×10^9 LtP/mL. The derived coupling constants can be assigned to the presence of a DMPO/•C adduct (100 %).

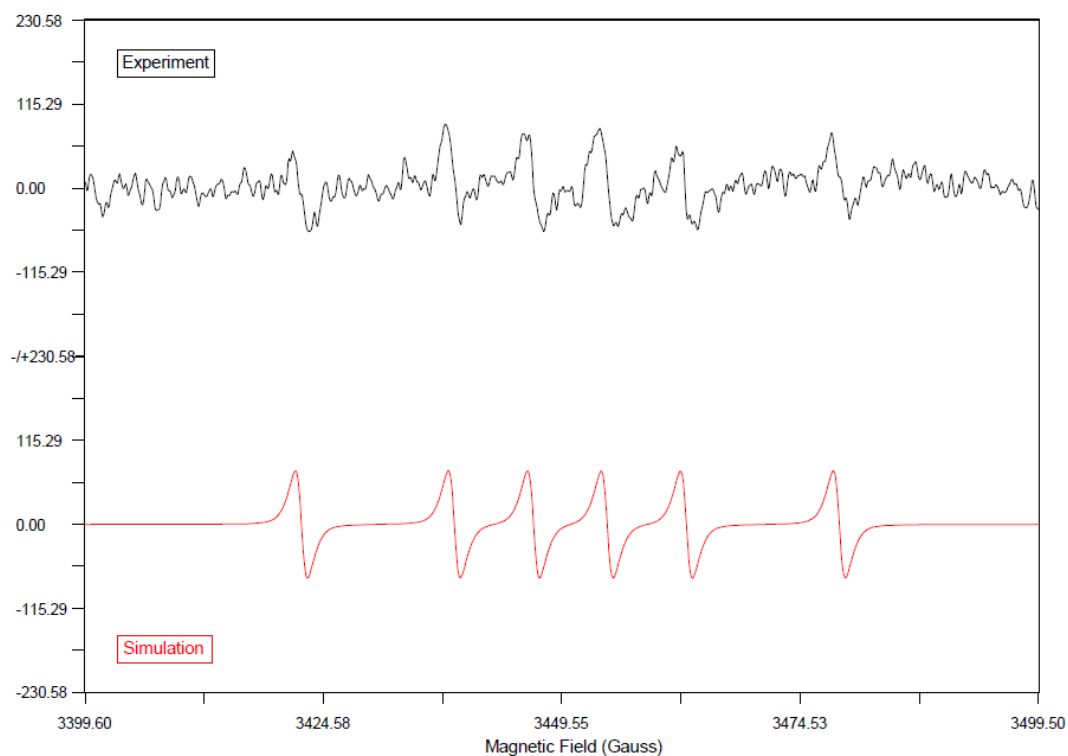


Fig. 28: EPR spectrum recorded after incubation of 599 μ M Asc with 2×10^9 LtP/mL in the presence of 40 mM DMPO in PBS/Glucose (15 mM) and the corresponding simulated spectrum generated with the WINSIM software. The coupling constants obtained from this simulation $a_N = 16$ G and $a_H = 24.3$ G suggest the presence of a DMPO/•C adduct.

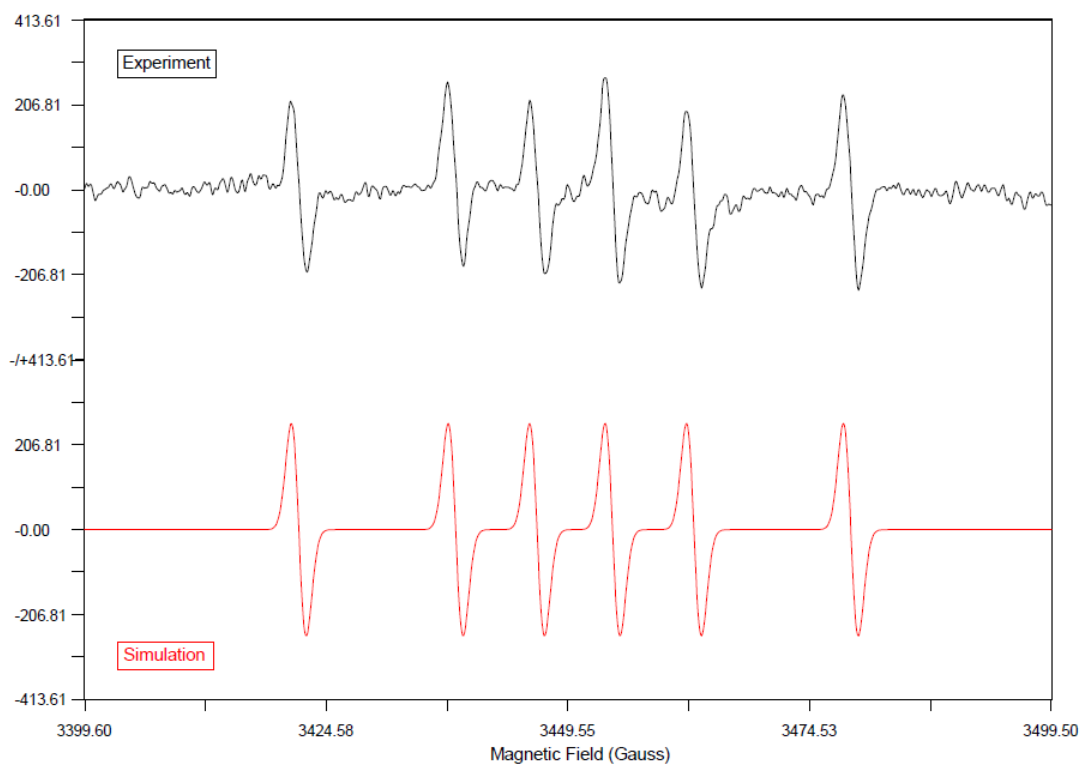


Fig. 29: EPR spectrum recorded after incubation of 599 μM Asc with 4×10^9 LtP/mL in the presence of 40 mM DMPO in PBS/Glucose (15 mM) and the corresponding simulated spectrum generated with the WINSIM software. The coupling constants obtained from this simulation $a_N = 16.2$ G and $a_H = 24.6$ G suggest the presence of a DMPO/ $^{\bullet}\text{C}$ adduct.

To follow the development of the DMPO/•C and DMPO/•OH adduct, we measured the Ipp every 40 min over six timepoints. The time course of the EPR signal intensities for the DMPO/•C and DMPO/•OH adducts for Asc in the presence of DMPO and 2×10^9 LtP/mL are shown in Fig. 30 and its control samples without Asc in Fig. 31. In comparison, Fig. 32 shows the results of the same experiment, but with 4×10^9 LtP/mL and Fig. 33 its control samples without Asc.

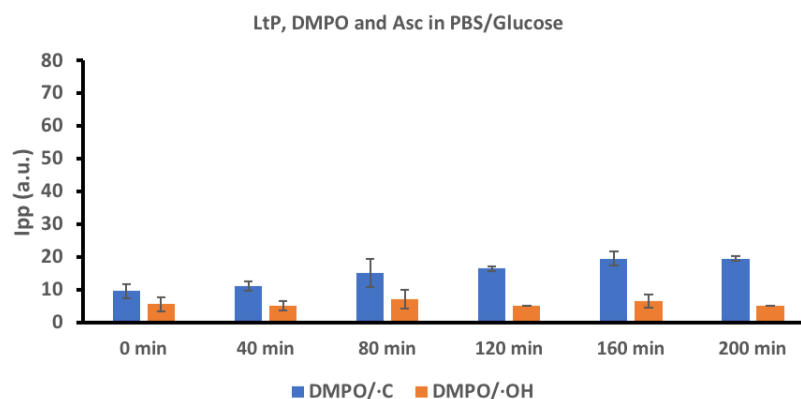


Fig. 30: Time-dependent development of the DMPO/•C and DMPO/•OH adduct intensities (Ipp) in 200 µL PBS/Glucose (15 mM) with 2×10^9 LtP/mL, 40 mM DMPO and 599 µM Asc. Samples were measured after incubation for 0 min, 40 min, 80 min, 120 min, 160 min or 200 min at 26.5 °C with constant agitation (speed: 0.3 s⁻¹). Data represent mean ± SD (n = 2).

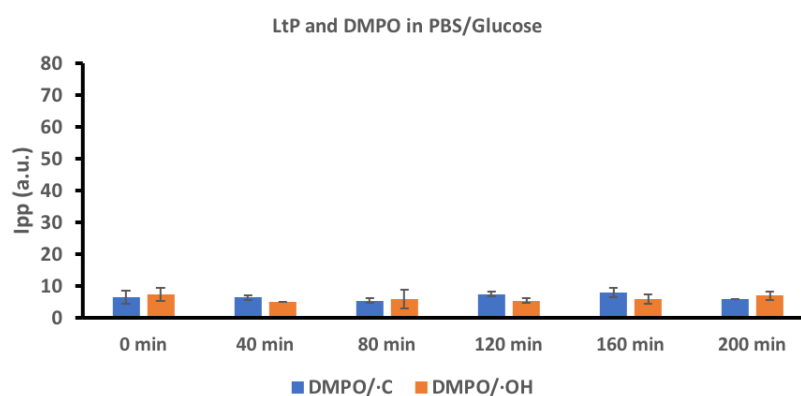


Fig. 31: Time-dependent development of the DMPO/•C and DMPO/•OH adduct intensities (Ipp) in 200 µL PBS/Glucose (15 mM) with 2×10^9 LtP/mL and 40 mM DMPO. Samples were measured after incubation for 0 min, 40 min, 80 min, 120 min, 160 min or 200 min at 26.5 °C with constant agitation (speed: 0.3 s⁻¹). Data represent mean ± SD (n = 2).

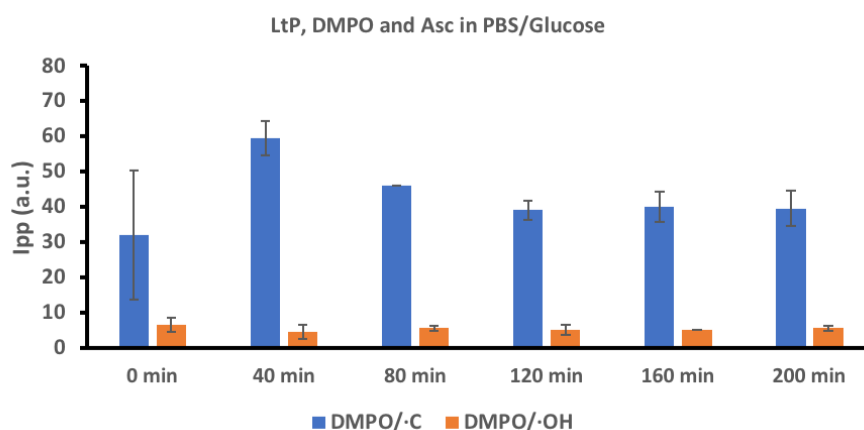


Fig. 32: Time-dependent development of the DMPO/[•]C and DMPO/[•]OH adduct intensities (Ipp) in 200 µL PBS/Glucose (15 mM) with 4×10^9 LtP/mL, 40 mM DMPO and 599 µM Asc. Samples were measured after incubation for 0 min, 40 min, 80 min, 120 min, 160 min or 200 min at 26.5 °C with constant agitation (speed: 0.3 s⁻¹). Data represent mean ± SD (n = 2).

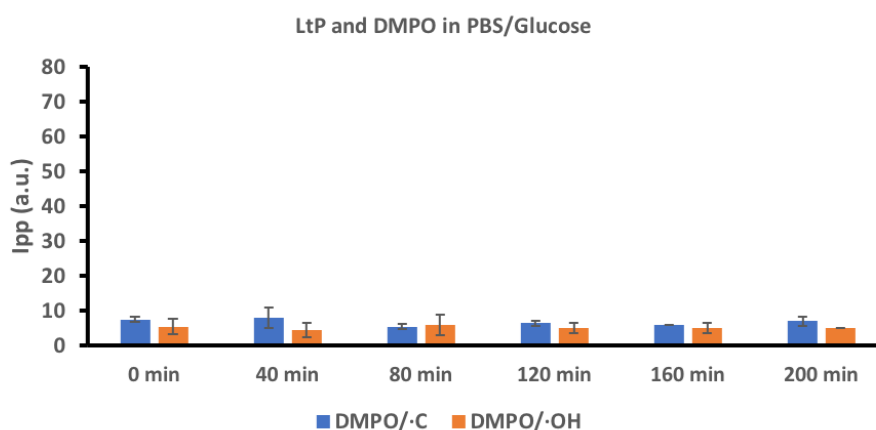


Fig. 33: Time-dependent development of the DMPO/[•]C and DMPO/[•]OH adduct intensities (Ipp) in 200 µL PBS/Glucose (15 mM) with 4×10^9 LtP/mL and 40 mM DMPO. Samples were measured after incubation for 0 min, 40 min, 80 min, 120 min, 160 min or 200 min at 26.5 °C with constant agitation (speed: 0.3 s⁻¹). Data represent mean ± SD (n = 2).

The EPR signal intensities measured for the DMPO/[•]C adducts are significantly higher with a cell number of 4×10^9 LtP/mL (Fig. 32) than in experiments with 2×10^9 LtP/mL (Fig. 30). For both experiments, the signal intensities are quite stable over the measurement time. No DMPO/[•]OH adducts were detected and DMPO/[•]C adducts were not measured in all control samples (Fig. 31 and 33).

3.2.2.2. Art-derived radicals in LtP

Furthermore, experiments with Art in LtP were performed. Art was incubated with 2×10^9 LtP/mL and DMPO in PBS/Glucose over different durations. Due to the longer reaction time of Art and its poor solubility, samples were measured over 72 h and the results are shown in Fig. 34. No signals for DMPO/ \cdot C and DMPO/ \cdot OH adducts were detected. The results for the control samples without Art are shown in Fig. 35 and also no spin adducts were observed.

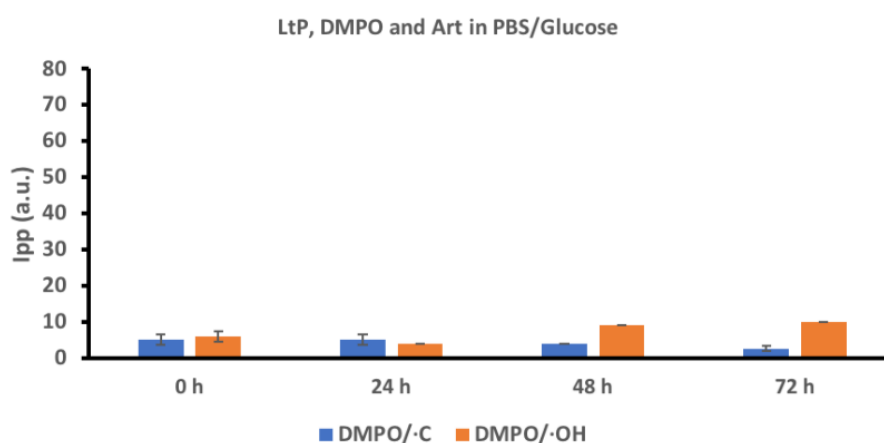


Fig. 34: Time-dependent development of the DMPO/ \cdot C and DMPO/ \cdot OH adduct intensities (Ipp) in 200 μ L PBS/Glucose (15 mM) with 2×10^9 LtP/mL, 40 mM DMPO and 756 μ M Art. Samples were frozen at 0 h, 24 h, 48 h, and 72 h and measured after 10 min incubation at room temperature. Data represent mean \pm SD (n = 2).

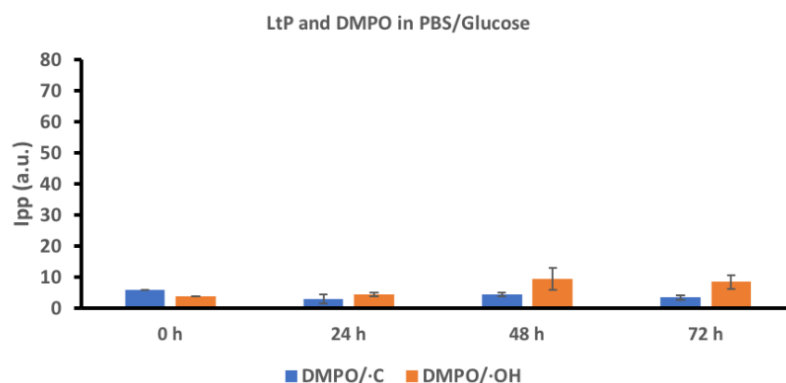


Fig. 35: Time-dependent development of the DMPO/[•]C and DMPO/[•]OH adduct intensities (Ipp) in 200 µL PBS/Glucose (15 mM) with 2×10^9 LtP/mL and 40 mM DMPO. Samples were frozen at 0 h, 24 h, 48 h, and 72 h and measured after 10 min incubation at room temperature. Data represent mean \pm SD (n = 2).

3.2.3. Spin trapping of lipid-derived radicals in LtP and model systems

There is sufficient evidence that EPs form drug-derived primary radicals in *Leishmania*. Based on different experimental endpoints we know that these radicals impair the viability of *Leishmania*. From the fact that antioxidants can prevent the action of EPs on *Leishmania*, it was expected that primary drug-derived radicals give rise to secondary radicals derived from the interaction with biological components of *Leishmania*. Although there is a variety of possible secondary radicals, we focused on the possibility of the appearance of lipid-derived radicals. According to (Janzen et al. 1982, Trudell 1987, Qian et al. 2000), a procedure for the extraction of lipid-derived spin adducts was established. In the following figures, some of the experimental results were displayed.

In a first step, 250 μL aliquots of mixtures containing the spin trap DMPO were extracted and analyzed by EPR. As can be seen in Tab. 10 EPR signals of spin adducts after 30 min incubation are rather weak. At later time points the signals were more intense. The resulting EPR signals were rather complex and difficult to interpret. Especially, there was no considerable difference between the *Leishmania* group with and without Asc. Furthermore, also signals from samples containing the LA instead of *Leishmania* looked only slightly different. Additionally, we made samples with PBS/Glucose as a negative control for the samples containing LtP. Also, the control sample gave similar EPR splitting patterns.

Tab. 10: EPR spectra of extracted lipophilic DMPO spin adducts in LtP with Asc and without Asc, in model systems (LA) and control samples in PBS/Glucose. Samples were extracted with MeOH/CH₂Cl₂ and measured in EtOAc after 0.5 h, 1.5 h, 2.5 h and 3.5 h. (SA = volume and compounds of the sample for extraction, TRE = additional treatment, EX = extraction volume and compounds, EPR = final volume and solution for EPR measurement, TI = incubation time of the samples before extraction).

SA:	250 μL PBS/Glu (15 mM), LtP (2000 Mio/mL), DMPO (40 mM), Asc (600 μM)	250 μL PBS/Glu (15 mM), LtP (2000 Mio/mL), DMPO (40 mM)	250 μL PBS, LA (5 mM), DTPA (110 μM), DMPO (40 mM), FeSO ₄ (100 μM)	250 μL PBS/Glu (15 mM), DMPO (40 mM)
TRE:	-	-	-	-
EX:	4.5 mL MeOH/CH ₂ Cl ₂ (1:2)	4.5 mL MeOH/CH ₂ Cl ₂ (1:2)	4.5 mL MeOH/CH ₂ Cl ₂ (1:2)	4.5 mL MeOH/CH ₂ Cl ₂ (1:2)
EPR:	100 μL EtOAc	100 μL EtOAc	100 μL EtOAc	100 μL EtOAc
TI				
0.5 h				
1.5 h				
2.5 h				
3.5 h				

In a next step we increased the sample volume which was extracted from 250 μL to 1000 μL per sample. Because of the weak signal at the timepoints in Tab. 10, we focused on the 2 h and 3 h timepoint and dried the sample with a few grains of MgSO_4 before measurement. As a result, EPR spectra had an improved signal-to-noise ratio. Tab. 11 shows that, under these conditions in the *Leishmania* group with Asc additional lines on the outer border of the spectra of carbon-centered spin adducts became visible at 3 h (Tab. 11, blue dots), which were not seen in the control group without Asc. However, the remaining signal was still complex and also appeared in the dried control samples.

Tab. 11: EPR spectra of extracted lipophilic DMPO spin adducts in LtP with Asc and without Asc and in control samples without LtP. Samples were extracted with $\text{MeOH}/\text{CH}_2\text{Cl}_2$ and measured in EtOAc after 2 h or 3 h incubation time. EPR lines labeled with a blue dot can be assigned to a DMPO/C adduct.

SA:	1000 μL PBS/Glu (15mM), LtP (2000 Mio/mL), DMPO (40 mM), Asc (600 μM)	1000 μL PBS/Glu (15 mM), LtP (2000 Mio/mL), DMPO (40 mM)	1000 μL PBS/Glu (15 mM), DMPO (40 mM)	1000 μL PBS, DMPO (40 mM)
TRE:	dried with MgSO_4	dried with MgSO_4	dried with MgSO_4	dried with MgSO_4
EX:	4.5 mL $\text{MeOH}/\text{CH}_2\text{Cl}_2$ (1:2)	4.5 mL $\text{MeOH}/\text{CH}_2\text{Cl}_2$ (1:2)	4.5 mL $\text{MeOH}/\text{CH}_2\text{Cl}_2$ (1:2)	4.5 mL $\text{MeOH}/\text{CH}_2\text{Cl}_2$ (1:2)
EPR:	100 μL EtOAc	100 μL EtOAc	100 μL EtOAc	100 μL EtOAc
TI				
2 h				
3 h				

In subsequent experiments for samples containing *Leishmania*, cells were sedimented prior to extraction and the amount of Asc was increased. Although EPR spectra from *Leishmania*-containing samples in this experiment differed from the buffer control experiments, the EPR splittings were difficult to interpret and showed no difference between Asc group versus the non-Asc group (Tab. 12). Likewise, in the control experiments without *Leishmania* strong EPR signals were observed.

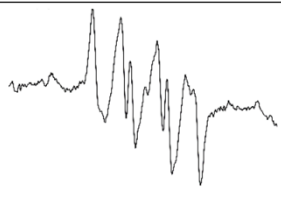
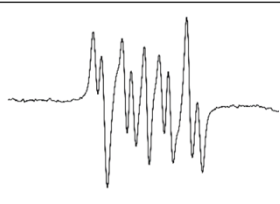
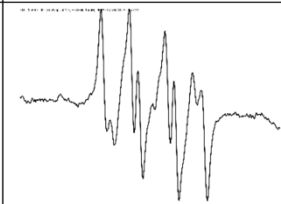
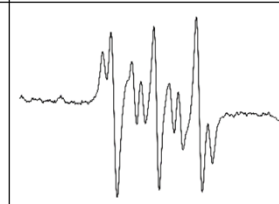
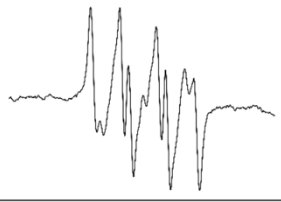
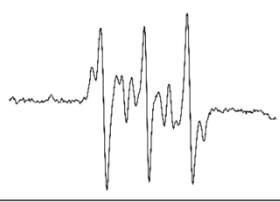
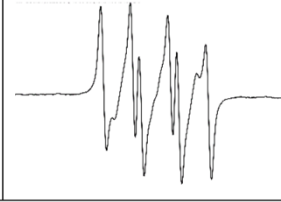
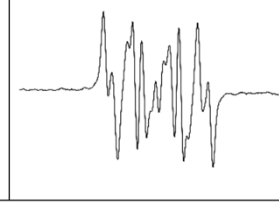
Tab. 12: EPR spectra of extracted lipophilic DMPO spin adducts in LtP with Asc, without Asc and in control samples without LtP. Samples containing LtP were centrifuged and resuspended in fresh PBS before extraction. Samples were extracted with MeOH/CH₂Cl₂ and measured in EtOAc after 2 h or 3 h incubation time.

SA:	1000 μ L PBS/Glu (15 mM), LtP (2000 Mio/mL), DMPO (40 mM), Asc (1000 μ M)	1000 μ L PBS/Glu (15 mM), LtP (2000 Mio/mL), DMPO (40 mM)	1000 μ L PBS/Glu (15 mM), DMPO (40 mM)	1000 μ L PBS, DMPO (40 mM)
TRE:	centrifuged and resuspended in new PBS before extraction	centrifuged and resuspended in new PBS before extraction	-	-
EX:	4.5 mL MeOH/CH ₂ Cl ₂ (1:2)	4.5 mL MeOH/CH ₂ Cl ₂ (1:2)	4.5 mL MeOH/CH ₂ Cl ₂ (1:2)	4.5 mL MeOH/CH ₂ Cl ₂ (1:2)
EPR:	100 μ L EtOAc	100 μ L EtOAc	100 μ L EtOAc	100 μ L EtOAc
TI				
2 h				
3 h				

Since the results so far suggested an impurity in the spin trap DMPO, which is extracted under these conditions, we performed more control experiments.

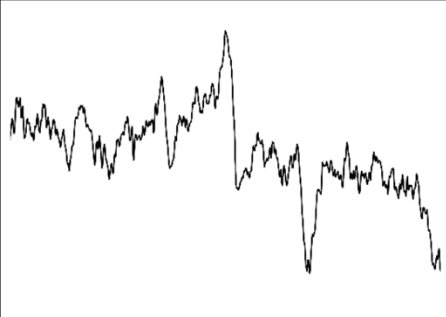
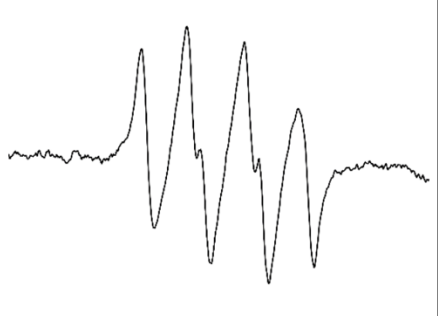
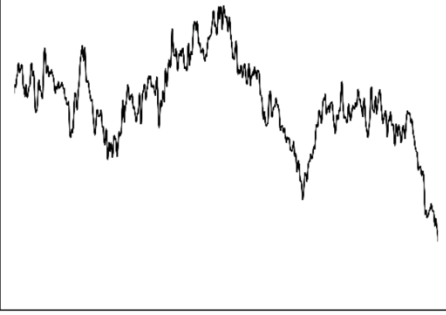
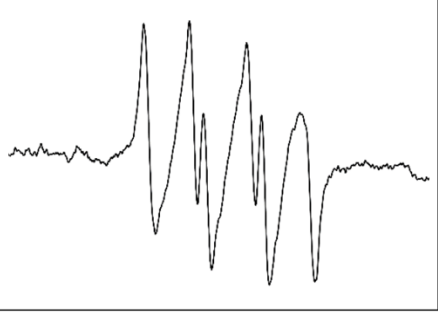
For this purpose, DMPO solutions in PBS with and without glucose were pretreated with activated charcoal to remove possible lipophilic impurities. In addition, extraction was performed with chloroform (CHCl₃) instead of dichloromethane (CH₂Cl₂). Unfortunately, as shown in Tab. 13, pretreatment with activated charcoal did not remove the impurities from DMPO. However, we observed that using chloroform in the organic extraction mixture slightly improved spectral resolution of the EPR spectra in comparison to dichloromethane.

Tab. 13: Control experiment in PBS or PBS/Glucose with DMPO and comparison of chloroform (CHCl_3) and dichloromethane (CH_2Cl_2). Samples were extracted and measured after an incubation time of 2 h and measured in duplicates.

SA:	1000 μL PBS, DMPO (40 mM)	1000 μL PBS, DMPO (40 mM)	1000 μL PBS/Glu (15 mM), DMPO (40 mM)	1000 μL PBS/Glu (15 mM), DMPO (40 mM)
TRE:	Treatment of PBS/DMPO with activated charcoal	Treatment of PBS/DMPO with activated charcoal	Treatment of PBS/DMPO with activated charcoal	Treatment of PBS/DMPO with activated charcoal
EX:	4.5 mL MeOH/ CH_2Cl_2 (1:2)	4.5 mL MeOH/ CHCl_3 (1:2)	4.5 mL MeOH/ CH_2Cl_2 (1:2)	4.5 mL MeOH/ CHCl_3 (1:2)
EPR:	100 μL EtOAc	100 μL EtOAc	100 μL EtOAc	100 μL EtOAc
TI				
2 h				
2 h				

As a final extraction experiment, we compared spin adducts extracted from PBS with and without DMPO (Tab. 14). Samples were again pretreated with a few grains MgSO_4 before measurement. Although some noisy background signal was observed in the extractions from PBS only, it is clearly visible that the major signal of the impurities only appears in the presence of DMPO.

Tab. 14: Control experiment in PBS with and without DMPO. Samples were extracted with MeOH/CH₂Cl₂ and measured in EtOAc after an incubation time of 2 h in duplicates.

SA:	1000 μ L PBS	1000 μ L PBS, DMPO (40 mM)
TRE:	dried with MgSO ₄	dried with MgSO ₄
EX:	4.5 mL MeOH/CH ₂ Cl ₂ (1:2)	4.5 mL MeOH/CH ₂ Cl ₂ (1:2)
EPR:	100 μ L EtOAc	100 μ L EtOAc
TI		
2 h		
2 h		

4. Discussion

4.1. Drugs against leishmaniasis

Even though some antileishmanial drugs are available, they can result in severe side effects, high costs or lack of efficacy (Zulfiqar et al. 2017). Therefore, the development of new drugs to treat the infection gains higher significance. Moreover, depending on the *Leishmania spp.* and immunological response different clinical manifestations (Tab. 1) can occur, which need individual treatment and because of that, a lot of research for new antileishmanial compounds and their efficacy is required (Kaye and Scott 2011).

4.2. EPs against leishmaniasis

During research for treatment options against intracellular protozoal pathogens, EPs showed promising results for being new optional drug candidates. For example, Art is successfully used as an antimalarial drug against *Plasmodia* (Wang et al. 2015). Also, for leishmaniasis treatment studies with Art were done. Nevertheless, its specific mechanism of action in *Leishmania* is quite complex and different from its action in *Plasmodia*. Both, *Leishmania* and *Plasmodia* are dependent on the heme/iron supply by their host cells, but it remained unclear how the efficiency of Art against *Leishmania* is influenced by mechanisms involved in iron uptake or metabolism (Geroldinger et al. 2020).

Moreover, a previous study showed that the EP Asc is effective against *Leishmania in vitro* and *in vivo*. For example, Asc was successfully used for the treatment of cutaneous leishmaniasis in a mouse model. Asc reduced the lesion size more effectively than other antileishmanial drugs in this model (Geroldinger et al. 2017).

Other promising candidates are EPs derived from anthracene, which are chemically synthesized. A previous study showed that certain anthracene EPs kill *Leishmania in vitro* (Geroldinger et al. 2018), have antileishmanial properties and are less toxic against macrophages (Piontek 2019).

4.3. Activation of Asc and Art

In spite of the clinical utilization of Art against malaria, its molecular mechanism in this disease is still matter of debate. For the malaria parasite residing in erythrocytes, a dual mechanism of Art was proposed. On the one hand it was suggested that Art is activated by heme from hemoglobin degradation of the parasite and on the other hand it was proposed

that Art is activated by intermediates of heme synthesis in the *Plasmodia* parasites (Wang et al. 2015).

For the action of EPs in *Leishmania*, we found that the actual activation mechanism of an EP strongly depends on its molecular structure beyond the EP group. For Asc, which is a rather low molecular EP derived from terpene compounds, it was demonstrated that it is preferably activated by the labile iron pool in *Leishmania* (Geroldinger et al. 2017). In contrast for Art in *Leishmania*, it was shown that heme as a binding partner and activator plays a major role. Furthermore, it was observed that Art possibly interferes in the heme degradation in *Leishmania* (Geroldinger et al. 2020).

These different studies confirmed that in general EPs require activation to the corresponding radicals to exert their pharmacological action although activation pathways and interacting biological molecules might be different.

4.4. Basic mechanism of EPs and experimental evidence

This evidence derives from different experimental approaches. For Asc, we have been able to detect its carbon-centered (primary) radicals directly in *Leishmania*. In contrast, for Art this was not successful in *Leishmania* so far. Another line of evidence for the presence and importance of radical intermediates comes from the interference of antioxidants and spin traps in the antileishmanial action of EPs. In the current work we observed that Asc and Art are active against LtP with IC₅₀ values in the μM range (Fig. 8, Tab. 8). Furthermore, the interference of DMPO in the antileishmanial activity of Asc and Art (Tab. 9) was found. Similar results were obtained in previous studies for a variety of natural and synthetic EPs (Geroldinger et al. 2017). Usually, this interference leads to an increase of IC₅₀ values for *Leishmania* viability in the presence of these antioxidants or radical scavengers compared to control experiments without these compounds. However, there is a big discrepancy between these interference experiments and direct detection of drug-derived radicals by EPR spectroscopy. For many EPs we demonstrated in the past the interference of antioxidants and radical scavengers in the antileishmanial action, however, for only a few of these compounds a direct detection of the EP-derived radical was possible (Tab. 6). This was an important starting point for the current work with the aim to explore the conditions which enable or disable radical detection from activation of Asc and Art.

4.4.1. Biomimetic system: H₂O₂

In a first step, we studied the formation of hydroxyl radicals from H₂O₂, as a prototype of a peroxide, and their spin trapping by DMPO. Using water as solvent Fe²⁺ triggered the formation of hydroxyl radicals from H₂O₂ as shown in Fig. 9 and 10. In our experiments, different ratios of H₂O₂ to iron were tested for the resulting intensity of the spin adduct and its persistence over ten minutes (Fig. 11). Surprisingly the equimolar ratio of one to one for H₂O₂ and iron did not give the highest signals. In contrast, ratios with a lower amount of iron, such as 5:1 or 10:1 gave higher signal intensities and signals of spin adducts were more stable over time (Figs. 12 and 13). According to literature (Fontmorin et al. 2016), this is due to the fact that Fe³⁺, which is formed in the reaction of peroxides with Fe²⁺, can react with the resulting DMPO/•OH spin adducts forming diamagnetic products and thereby declining the EPR signal intensity. However, the situation in PBS was completely different since for all tested H₂O₂:Fe²⁺ ratios the 1:1 ratio gave the highest signal which was also rather stable over ten minutes, as displayed in Fig. 14. This suggests that Fe³⁺, which in water is responsible for the decline of the EPR signal, is obviously complexed by phosphate in PBS decreasing its reactivity. Therefore, in PBS solutions it was observed that increasing amounts of Fe²⁺ generate increasing amounts of radicals from peroxides up to equimolar ratios. In addition, DMPO/•OH spin adduct intensities in water were in most cases higher than for the corresponding experiments in PBS, demonstrating that phosphate obviously also diminishes the redox activity of Fe²⁺.

4.4.2. Biomimetic system: Asc

In this study, similar experiments with Asc and its activation by Fe²⁺ were performed. In water spin adducts of carbon-centered radicals (DMPO/•C) were detected as major product and DMPO/•OH adducts as side product (Figs. 15 and 16). In contrast, compared to H₂O₂ the intensity of carbon-centered DMPO adducts continuously increased with increasing amounts of Fe²⁺ (Fig. 17) in water, while DMPO/•OH adducts were stable over the time (Fig. 18). Therefore, it was concluded that Fe³⁺ formed in the course of this reaction, apparently reacts quickly with DMPO/•OH adducts but not with DMPO/•C adducts. Repeating these experiments with Asc and Fe²⁺ in PBS (Figs. 19 and 20) it was observed that also in this system a higher amount of Fe²⁺ generated more DMPO/•C adducts as displayed in Fig. 21. However, signal intensities of these DMPO/•C adducts in PBS were lower than in water for corresponding conditions. No DMPO/•OH adducts were detected under these conditions.

4.4.3. Biomimetic system: Art

For Art it is even harder to detect carbon-centered radicals in these systems due to its lower reactivity and lower water solubility in comparison to Asc. Nevertheless, in this study we succeeded for the first time to detect Art-derived radicals with DMPO in the absence of significant amounts of organic solvents (Fig. 22). Similar to the other experiments in water, DMPO/•OH adducts were detected as side products in both samples with Art (Fig. 22) and without Art (Fig. 23). Observing the Ipp development of DMPO/•C and DMPO/•OH adducts over 48 h the DMPO/•C intensity over the first 24 h was quite stable and decreased afterwards (Figs. 24 and 25).

However, corresponding experiments in PBS failed to detect the Art-derived carbon-centered radicals (Figs. 26 and 27).

The results of this work clearly demonstrate that factors which influence the outcome of those EPR experiments are already present in the absence of *Leishmania* in a simple biomimetic system. As we have seen for Asc and Art, the radical formation in the presence of Fe²⁺ is already different between water and PBS as solvent. In PBS the formation of carbon-centered radicals from these EPs is significantly retarded in comparison to water as solvent. This could have two reasons. On the one hand, phosphate in PBS could bind Fe²⁺ and/or Fe³⁺ and, therefore, could influence the ability of Fe²⁺ to reduce the peroxide bond in the respective EPs. Another factor, especially for the larger EP Art, is that PBS solutions have much higher ionic strength than water and, therefore, could reduce the water solubility of complex EPs, such as Art.

4.4.4. Biological system (LtP): Asc and Art

In *Leishmania* suspensions, we successfully detected carbon-centered radicals as DMPO/•C derived from Asc with different cell numbers (Figs. 28–33).

Corresponding experiments for Art in *Leishmania* did not result in detectable amounts of DMPO/•C spin adducts (Figs. 34 and 35). As already mentioned above, this could already be caused by using PBS as a solvent for *Leishmania*.

4.5. Extraction of lipid-derived spin adducts

This is one reason why the last experimental part of this work focused on the extraction of lipid-derived radical DMPO spin adducts, which were suggested to be enriched during extraction and should exhibit a higher stability in organic solvents (Janzen et al. 1982, Trudell

1987, Qian et al. 2000). Tab. 15 shows coupling constants of DMPO spin adducts in ethyl acetate. In comparison to coupling constants of corresponding spin adducts in water, there are significant differences: (i) coupling constants are quantitative different between water and ethyl acetate and (ii) in ethyl acetate in addition to H β couplings H γ couplings are also often observed. This additional information might be helpful for assignments of signals to certain spin adducts.

Tab. 15: Coupling constants (a_N , a_H (β), a_H (γ)) of DMPO spin adducts in ethyl acetate (Qian et al. 2000, Venkataraman et al. 2004). (d_H = line width, Lor/Gauss = ratio of Lorentzian and Gaussian lineshape)

Radical	Solvent	a_N (G)	a_H (β) (G)	a_H (γ) (G)	d_H (G)	Lor/Gauss
DMPO/Ld \cdot	EtOAc	13.50	10.20	-	1.30	0.70
DMPO/LO \cdot	EtOAc	12.80	6.85	1.90	1.10	0.50
DMPO/LOO \cdot (L10 \cdot)	EtOAc	13.13	10.59	1.34	-	-
DMPO/L20 \cdot	EtOAc	13.28	6.88	2.00	-	-
DMPO/OL \cdot	EtOAc	13.74	8.75	1.83	-	-
DMPO/ \cdot OOH	EtOAc	13.00	10.50	-	-	-
DMPO/ \cdot OH	EtOAc	13.70	10.40	-	-	-
DMPO/X \cdot	EtOAc	14.05	12.16	-	-	-

Although our efforts to extract lipophilic spin adducts from samples containing *Leishmania*, DMPO and unsaturated fatty acids in the presence of iron were successful, a meaningful assignment of the EPR signals to lipid-derived radicals was impossible (Tab.10, 11, 12). The major reason for this negative result was that our current DMPO preparation apparently contained already lipophilic spin adducts or their precursors (Tab. 14).

Usually, DMPO stock solutions are prepared from commercially available DMPO with purities of 97 to 98 %. Preparations of DMPO stocks in water includes bubbling of the solvent with nitrogen to remove oxygen and results in stock solutions with concentrations above 1000 mM. To remove possible impurities these solutions are treated with activated charcoal, which usually removes lipophilic compounds responsible for the light-yellow color of the stock solutions. This also corresponds to an increased UV absorption (Janzen et al. 1989). Due to this treatment, it is usually achieved that DMPO dilutions in normal experimental

concentrations of around 40 to 50 mM do not show any residual signal in the EPR spectrum. This quality criterion was met by all DMPO stocks used in this study. Apparently, this purification procedure for DMPO stocks is not sufficient for the lipophilic spin adduct extraction experiments (Tab. 13). Possible reasons could be that this extraction procedure favors the accumulation of lipophilic compounds in the organic phase including lipophilic DMPO impurities. Furthermore, the strong reduction of the volume by this procedure (sample volume 1000 μL of PBS suspension, EPR measurement volume 100 μL in ethyl acetate) further favors the concentration of these background spin adducts. This gave rise to high-intensity EPR signals, which overlap and hide all other spin adducts generated in our test systems. We tried to circumvent this problem by extraction of the PBS/DMPO solutions with activated charcoal after sample preparation, but this resulted in no significant resolution of the background problem.

4.6. Practical conclusion

Although PBS is commonly used as solvent for cells in biological systems, it seems to be a difficult choice for detection of EP-derived radicals by spin trapping. Of course, these experiments cannot be conducted in water due to the lack of osmotic support for the cells in this environment. However, in future alternative buffer systems without phosphate for this purpose could be of interest, such as 3-(N-morpholino)propanesulfonic acid (MOPS) or 4-(2-hydroxyethyl)-1-piperazineethanesulfonic acid (HEPES) buffers (Tadolini 1987a, 1987b, Tadolini and Sechi 1987). Extraction of lipophilic DMPO spin adducts seems to be still promising because of the increased sensitivity and stability of the spin adducts as well as the possible access to secondary radical intermediates, such as lipid peroxidation-derived radicals, which may appear downstream of primary EP actions. However, essential for this technique is the improved purification of DMPO stocks. Besides activated charcoal treatment of DMPO stock solutions other possibilities are vacuum distillation of neat DMPO prior to dissolution in water (Buettner 1985), benzene extraction of DMPO stocks (Kotake et al. 1994) or chromatographic purification of aqueous DMPO stock solutions (Stolze et al. 2002).

4.7. General conclusions

This work demonstrates that detection of radical intermediates in cells and other biological systems is difficult and strongly depends on experimental conditions. A major consequence of this observation is that for EPR experiments in these systems numerous control experiments are required. Furthermore, even with optimized conditions detection of radical

intermediates from EPs by DMPO, spin trapping will be only successful in specifically designed experimental conditions, which cannot completely match conditions used for viability assays (especially with respect to the cell number/mL and the drug/cell ratio). Therefore, always a multitude of approaches is required to reliably illustrate the involvement of drug-derived radicals in the pharmacological actions of EPs. This underlines the importance of EPR spin trapping since in contrast to many other methods this EPR method is prone to false negatives but much less to false positive results, which is important for the mechanistic interpretations of the findings.

5. Summary

Leishmaniasis is one of the most important tropical diseases caused by different protozoal species of the genus *Leishmania* with the sand fly as their vector. There are about two million new cases and 70.000 deaths per year due to this disease. Because of climate change and spreading of the sand fly vector, these numbers will increase in the future also in previously non-endemic areas. Although some treatment options are available, an affordable, effective and safe treatment is difficult to find. This is due to resistance development, side effects and high costs of drugs. Thus, there is a high need of new treatment options against leishmaniasis. In the recent years, it was shown that endoperoxides are potentially suitable to treat leishmaniasis and that their activation to radicals is essential for their pharmacological activity. For some endoperoxides, such as ascaridole, the formation of primary radicals was detected in both biomimetic systems and in *Leishmania tarentolae* promastigotes by electron paramagnetic resonance spectroscopy. However, even for some highly active endoperoxides radical detection by electron paramagnetic resonance spectroscopy in *Leishmania* often was not successful, despite radical scavengers had a clear negative effect on the antileishmanial activity of these endoperoxides. So far, only a few drug-derived (primary) radicals of endoperoxides have been detected and identified by using DMPO as spin trap in biomimetic systems and in *Leishmania* by electron paramagnetic resonance spectroscopy. In this work we showed in biomimetic systems that radical detection from endoperoxides (ascaridole and artemisinin) and H_2O_2 by electron paramagnetic resonance spin trapping is already dependent on buffer composition, time points and subsequent reactions of the spin adducts. For the first time in an aqueous system without significant amounts of organic solvents, the detection of radicals from artemisinin triggered by Fe^{2+} was achieved by electron paramagnetic resonance spin trapping. In cellular *Leishmania tarentolae* promastigotes suspensions primary radicals derived from the endoperoxide ascaridole but not from the endoperoxide artemisinin were detected by electron paramagnetic resonance spin trapping. Furthermore, this study established an extraction procedure for lipophilic spin adducts. However, identification of extracted spin adducts was impaired by a strong background signal, which arose from impurities in the spin trap itself.

This work provides a more systematic understanding of electron paramagnetic resonance spin trapping results from activated endoperoxides and gives inspirations for future experiments.

6. Zusammenfassung

Leishmaniose ist eine der wichtigsten tropischen Krankheiten mit der Sandmücke als Vektor. Sie wird durch verschiedene Spezies der Gattung *Leishmania* verursacht. Jährlich erkranken schätzungsweise zwei Millionen Menschen an Leishmaniose und ungefähr 70.000 sterben daran. Aufgrund der globalen Erwärmung und der damit verbundenen Ausbreitung der Sandmücke bis in Gebiete, in denen sie momentan noch nicht vorzufinden ist, werden diese Zahlen in der Zukunft ansteigen. Derzeit gibt es bereits einige Behandlungsoptionen, aber die gegenwärtigen Therapiemöglichkeiten sind limitiert, aufgrund von Resistenzentwicklungen, starken Nebenwirkungen aber auch hohen Kosten der Medikamente. Daher besteht ein hoher Bedarf an neu entwickelten Wirkstoffen gegen Leishmaniose. In den letzten Jahren wurde gezeigt, dass Endoperoxide mögliche Kandidaten für eine Behandlung von Leishmaniose sind und dass ihre Aktivierung in Verbindung mit Radikalbildung wichtig für ihre pharmakologische Aktivität ist. Für Endoperoxide, wie beispielsweise Ascaridol wurde die Bildung von primären Radikalen sowohl im biomimetischen System als auch in *Leishmania tarentolae* Promastigoten mittels Elektronenspinresonanz Spektroskopie nachgewiesen. Radikale konnten jedoch oft für manche hochaktive Endoperoxide in *Leishmanien* nicht erfolgreich mittels Elektronenspinresonanz Spektroskopie nachgewiesen werden, obwohl Radikalfänger einen klaren negativen Effekt auf die antileishmaniale Aktivität dieser Endoperoxide zeigten. Bis jetzt konnten nur ein paar von Wirkstoffen abgeleitete (primäre) Radikale der Endoperoxide mittels Elektronenspinresonanz Spektroskopie unter der Verwendung von DMPO als Spin Trap sowohl im biomimetischen System als auch in *Leishmanien* detektiert und identifiziert werden. In dieser Arbeit wurde gezeigt, dass der Nachweis von Radikalen von Endoperoxiden (Ascaridol und Artemisinin) und H_2O_2 durch Elektronenspinresonanz Spin Trapping bereits im biomimetischen System von der Pufferzusammensetzung, den Messzeitpunkten und nachfolgenden Reaktionen der Spin Addukte abhängig ist. Zum ersten Mal wurde im wässrigen System ohne signifikante Zugabe von organischen Lösungsmitteln der Nachweis von Radikalen von Artemisinin, ausgelöst durch Fe^{2+} über Elektronenspinresonanz Spin Trapping erfolgreich durchgeführt. In Zellsuspensionen mit *Leishmania tarentolae* Promastigoten konnten nur primäre Radikale, abgeleitet von Ascaridol, nicht jedoch von Artemisinin mittels Elektronenspinresonanz Spin Trapping nachgewiesen werden. Darüber hinaus wurde in dieser Arbeit eine Methode für die Extraktion von lipophilen Spin Addukten etabliert. Die Identifikation der extrahierten Spin

Addukte wurde jedoch sehr von einem starken Hintergrundsignal beeinträchtigt, welches aufgrund der Verunreinigungen des Spin Traps selbst entstanden ist.

Diese Arbeit verschafft ein höheres systematisches Verständnis der Elektronenspinresonanz Spin Trapping Ergebnisse von aktivierten Endoperoxiden und bietet viele neue Ansatzpunkte für zukünftige Experimente.

7. Abbreviations

AcEP1117	...	anthracene endoperoxide 1117
AcEP1118	...	anthracene endoperoxide 1118
AcEP1129	...	anthracene endoperoxide 1129
AcEP1130	...	anthracene endoperoxide 1130
ALA	...	δ -aminolevulinic acid
ALogP	...	partition coefficient
AmB	...	amphotericin B
Arsu	...	artesunate
Art	...	artemisinin
Asc	...	ascariidole
BHI	...	brain heart infusion medium
BMPO	...	5-tert-butoxycarbonyl 5-methyl-1-pyrroline N-oxide
DBNBS	...	3,5-dibromo-4-nitrosobenzene sulfonic acid
DEMPO	...	5-diethoxyphosphoryl-5-methyl-1-pyrroline
d_H	...	line width
DHA	...	dihydroartemisinin
DMPO	...	5,5-dimethyl-1-pyrroline N-oxide
DPAcEP	...	1,8-diphenyl-15,16-dioxatetracyclo[6.6.2.02,7.09,14]hexadeca-2(7),3,5,9(14),10,12-hexaene
EMPO	...	5-(ethoxycarbonyl)-5-methyl-1-pyrroline N-oxide
EP	...	endoperoxide
EPR	...	electron paramagnetic resonance
EtOAc	...	ethyl acetate
FeCN	...	ferricyanide
HAccept	...	hydrogen acceptors
Hb	...	hemoglobin
HDonor	...	hydrogen donors
HEPES	...	4-(2-hydroxyethyl)-1-piperazineethanesulfonic acid
IL	...	interleukin
ISP	...	inhibitor of serine peptidase
LA	...	linolenic acid
LIP	...	labile iron point

logPow	...	octanol-water partition coefficient
Lor/Gauss	...	ratio of Lorentzian and Gaussian lineshape
LPG	...	lipophosphoglycan
LtP	...	<i>Leishmania tarentolae</i> promastigotes
MB359EP1	...	[3,4,5-triacetoxy-6-[12-tert-butyl-8-[3,4,5-triacetoxy-6-(acetoxymethyl)tetrahydropyran-2-yl]-9,10-dioxatricyclo[6.2.2.02,7]dodeca-2(7),3,5,11-tetraen-1-yl]tetrahydropyran-2-yl]methyl acetate
MNP	...	2-methyl-2-nitrosopropane
MonoGluAcEP	...	[3,4,5-triacetoxy-6-(15,16 dioxatetracyclo[6.6.2.02,7.09,14]hexadeca-2(7),3,5,9(14),10,12-hexaen-1-yloxy)tetrahydropyran-2-yl]methyl acetate
MOPS	...	3-(N-morpholino)propanesulfonic acid
mPyAcEP	...	3-[8-(3-pyridyl)-15,16-dioxatetracyclo[6.6.2.02,7.09,14]hexadeca-2(7),3,5,9(14),10,12-hexaen-1-yl]pyridine
mPyBuAcEP	...	3-[4-tert-butyl-8-(3-pyridyl)-15,16-dioxatetracyclo[6.6.2.02,7.09,14]hexadeca-2(7),3,5,9(14),10,12-hexaen-1-yl]pyridine
MW	...	molecular weight
OD	...	optical density
oOMeAcEP	...	1,8-bis(2-methoxyphenyl)-15,16-dioxatetracyclo[6.6.2.02,7.09,14]hexadeca-2(7),3,5,9(14),10,12-hexaene
oPyAcEP	...	2-[8-(2-pyridyl)-15,16-dioxatetracyclo[6.6.2.02,7.09,14]hexadeca-2(7),3,5,9(14),10,12-hexaen-1-yl]pyridine
oPy2C8AcEP	...	[1,8-bis(2-pyridyl)-15,16-dioxatetracyclo[6.6.2.02,7.09,14]hexadeca-2(7),3,5,9(14),10,12-hexaen-4-yl]methyl nonanoate
PBN	...	α -phenyl-N-tert-butyl nitron
PBS	...	phosphate buffered saline
POBN	...	α -(4-pyridyl-1-oxide)-N-tert-butyl nitron
PPIX	...	protoporphyrin IX
PSA	...	polar surface area
ROS	...	reactive oxygen species
RotBonds	...	rotatable bonds
WHO	...	World Health Organization
WS	...	water solubility

YEM ... yeast extract medium

1062MeAcEP ... 1-methyl-4-[8-(1-methylpyridin-1-ium-4-yl)-15,16-dioxatetracyclo
[6.6.2.02,7.09,14]hexadeca-2(7),3,5,9(14),10,12-hexaen-1yl]pyridin
-1-ium;trifluoromethanesulfonate

8. References

- Baptista MS, Wainwright M. 2011. Photodynamic antimicrobial chemotherapy (PACT) for the treatment of malaria, leishmaniasis and trypanosomiasis. *Brazilian Journal of Medical and Biological Research*, 44(1):1–10.
- Bates PA. 2007. Transmission of *Leishmania* metacyclic promastigotes by phlebotomine sand flies. *International Journal for Parasitology*, 37(10):1097–1106.
- Bethony JM, Cole RN, Guo X, Kamhawi S, Lightowers MW, Loukas A, Petri W, Reed S, Valenzuela JG, Hotez PJ. 2011. Vaccines to combat the neglected tropical diseases. *Immunological Reviews*, 239(1):237–270.
- Bolton JR, Borg DC, Swartz HM. 1972. *Biological applications of electron spin resonance*. London, New York: Wiley Interscience, 64–118.
- Borg DC. 1976. Applications of electron spin resonance in biology. In: Pryor WA, *Free Radicals in Biology*, Vol. 1. New York: Academic Press, 69–147.
- Buettner GR. 1985. Spin trapping of hydroxyl radical. In: Greenwald RA, *CRC Handbook of Methods for Oxygen Radical Research*, Vol. 3. Florida: CRC Press, 151–155.
- Buettner GR. 1987. Spin trapping: Electron-spin-resonance parameters of spin adducts. *Free Radical Biology & Medicine*, 3(4):259–303.
- Carvalho L, Luque-Ortega JR, Lopez-Martin C, Castanys S, Rivas L, Gamarro F. 2011. The 8-aminoquinoline analogue sitamaquine causes oxidative stress in *Leishmania donovani* promastigotes by targeting succinate dehydrogenase. *Antimicrobial Agents and Chemotherapy*, 55(9):4204–4210.
- Davies MJ. 2016. Detection and characterisation of radicals using electron paramagnetic resonance (EPR) spin trapping and related methods. *Methods*, 109:21–30.
- Dong Y, Vennerstrom JL. 2003. Mechanisms of in situ activation for peroxidic antimalarials. *Redox Report*, 8(5):284–288.
- Dorfman LM, Adams GE. 1973. Reactivity of the hydroxyl radical in aqueous solutions. *National Standard Reference Data Series*, 46:1–72.
- Dorlo TP, Balasegaram M, Beijnen JH, de Vries PJ. 2012. Miltefosine: A review of its pharmacology and therapeutic efficacy in the treatment of leishmaniasis. *Journal of*

- Antimicrobial Chemotherapy, 67:2576–2597.
- Dueñas-Romero AM, Loiseau PM, Saint-Pierre-Chazalet M. 2007. Interaction of sitamaquine with membrane lipids of *Leishmania donovani* promastigotes. *Biochimica et Biophysica Acta*, 1768(2):246–252.
- Duling DR. 1994. Simulation of multiple isotropic spin-trap EPR spectra. *Journal of Magnetic Resonance Series B*, 104(2):105–110.
- Dunay IR, Wing CC, Haynes RK, Sibley LD. 2009. Artemisone and artemiside control acute and reactivated toxoplasmosis in a murine model. *Antimicrobial Agents and Chemotherapy*, 53(10):4450–4456.
- Ellington SP, Strauss KE, Rosen GM. 2019. Spin trapping of free radicals in whole cells, isolated organs, and in vivo. In: Chow CK, *Cellular Antioxidant Defense Mechanisms*, Vol. 1. Florida: CRC Press, 232.
- Ferroglio E, Maroli M, Gastaldo S, Mignone W, Rossi L. 2005. Canine leishmaniasis, Italy. *Emerging Infectious Diseases*, 11(10):1618–1620.
- Fontmorin JM, Burgos Castillo RC, Tang WZ, Sillanpää M. 2016. Stability of 5,5-dimethyl-1-pyrroline-N-oxide as a spin-trap for quantification of hydroxyl radicals in processes based on Fenton reaction. *Water Research*, 99:24–32.
- Fritsche CLE. 2008. Untersuchungen zur optimalen Kultivierung von *Leishmania tarentolae* [Dissertation]. Halle (Saale): Martin-Luther-Universität Halle-Wittenberg.
- Fudickar W, Linker T. 2018. Release of singlet oxygen from aromatic endoperoxides by chemical triggers. *Angewandte Chemie International Edition*, 57(39):12971–12975.
- Geroldinger G, Tonner M, Hettegger H, Bacher M, Monzote L, Walter M, Staniek K, Rosenau T, Gille L. 2017. Mechanism of ascaridole activation in *Leishmania*. *Biochemical Pharmacology*, 132:48–62.
- Geroldinger G, Tonner M, Fudickar W, De Sarkar S, Dighal A, Monzote L, Staniek K, Linker T, Chatterjee M, Gille L. 2018. Activation of anthracene endoperoxides in *Leishmania* and impairment of mitochondrial functions. *Molecules*, 23(7):1680.
- Geroldinger G, Tonner M, Quirgst J, Walter M, De Sarkar S, Machín L, Monzote L, Stolze K, Catharina Duvigneau J, Staniek K, et al. 2020. Activation of artemisinin and heme

- degradation in *Leishmania tarentolae* promastigotes: A possible link. *Biochemical Pharmacology*, 173:113737.
- Ghorbani M, Farhoudi R. 2018. Leishmaniasis in humans: Drug or vaccine therapy?. *Drug Design, Development and Therapy*, 12:25–40.
- Hawkins CL, Davies MJ. 2014. Detection and characterisation of radicals in biological materials using EPR methodology. *Biochimica et Biophysica Acta - General Subjects*, 1840(2):708–721.
- Janzen EG, Coulter GA, Oehler UM, Bergsma JP. 1982. Solvent effects on the nitrogen and beta-hydrogen hyperfine splitting constants of aminoxyl radicals obtained in spin trapping experiments. *Canadian Journal of Chemistry*, 60:2725–2733.
- Janzen EG, Jandrisits LT, Shetty R V, Haire DL, Hilborn JW. 1989. Synthesis and purification of 5,5-dimethyl-1-pyrroline-N-oxide for biological applications. *Chemico-Biological Interactions*, 70:167–172.
- Kakhlon O, Cabantchik ZI. 2002. The labile iron pool: Characterization, measurement, and participation in cellular processes. *Free Radical Biology & Medicine*, 33(8):1037–1046.
- Karkamo V, Kaistinen A, Nareaho A, Dillard K, Vainio-Siukola K, Vidgren G, Tuoresmaki N, Anttila M. 2014. The first report of autochthonous non-vector-borne transmission of canine leishmaniosis in the Nordic countries. *Acta Veterinaria Scandinavica*, 56:84.
- Kaye P, Scott P. 2011. Leishmaniasis: Complexity at the host-pathogen interface. *Nature Reviews Microbiology*, 9(8):604–615.
- Kotake Y, Reinke LA, Tanigawa T, Koshida H. 1994. Determination of the rate of superoxide generation from biological systems by spin trapping: Use of rapid oxygen depletion to measure the decay rate of spin adducts. *Free Radical Biology and Medicine*, 17(3):215–223.
- Lipinski CA, Lombardo F, Dominy BW, Feeney PJ. 2001. Experimental and computational approaches to estimate solubility and permeability in drug discovery and development settings. *Advanced Drug Delivery Reviews*, 46:3–26.
- Manske M, Miotto O, Campino S, Auburn S, Zongo I, Ouedraogo J, Michon P, Mueller I, Su X, Amaratunga C, et al. 2012. Analysis of *Plasmodium falciparum* diversity in natural infections by deep sequencing. *Nature*, 487(7407):375–379.

- Mitra B, Andrews NW. 2013. Irony of fate: Role of iron-mediated ROS in Leishmania differentiation. *Trends in Parasitology*, 29(10):489–496.
- Monzote L, Stamberg W, Staniek K, Gille L. 2009. Toxic effects of carvacrol, caryophyllene oxide, and ascaridole from essential oil of *Chenopodium ambrosioides* on mitochondria. *Toxicology and Applied Pharmacology*, 240(3):337–347.
- Müllebnner A, Patel A, Stamberg W, Staniek K, Rosenau T, Netscher T, Gille L. 2010. Modulation of the mitochondrial cytochrome bc1 complex activity by chromanols and related compounds. *Chemical Research in Toxicology*, 23(1):193–202.
- Piontek M. 2019. Antileishmanial efficiency and mechanism of anthracene endoperoxides [Bachelor Thesis]. Vienna: University of Veterinary Medicine.
- Podinovskaia M, Descoteaux A. 2015. Leishmania and the macrophage: A multifaceted interaction. *Future Microbiology*, 10(1):111–129.
- Qian SY, Wang HP, Schafer FQ, Buettner GR. 2000. EPR detection of lipid-derived free radicals from PUFA, LDL, and cell oxidations. *Free Radical Biology & Medicine*, 29(6):568–579.
- Ricciotti E, Fitzgerald GA. 2011. Prostaglandins and inflammation. *Arteriosclerosis, Thrombosis, and Vascular Biology*, 31(5):986–1000.
- Robert A, Benoit-Vical F, Meunier B. 2005. Heme as trigger and target of the antimalarial peroxide artemisinin. In: Sessler, J et al., *Medicinal Inorganic Chemistry*, Vol 1. Washington DC: American Chemical Society, 281–294.
- Rotureau B, Morales MA, Bastin P, Späth GF. 2009. The flagellum-mitogen-activated protein kinase connection in Trypanosomatids: A key sensory role in parasite signalling and development? *Cellular Microbiology*, 11(5):710–718.
- Savjani KT, Gajjar AK, Savjani JK. 2012. Drug solubility: Importance and enhancement techniques. *ISNR Pharmaceutics*, 2012:1–10.
- Sentjurs M, Mason RP. 1992. Inhibition of radical adduct reduction and reoxidation of the corresponding hydroxylamines in in vivo spin trapping of carbon tetrachloride-derived radicals. *Free Radical Biology and Medicine*, 13:151–160.
- Singh N, Kumar M, Singh RK. 2012. Leishmaniasis: Current status of available drugs and

- new potential drug targets. *Asian Pacific Journal of Tropical Medicine*, 5(6):485–497.
- Stolze K, Udilova N, Nohl H. 2002. ESR analysis of spin adducts of alkoxy and lipid-derived radicals with the spin trap Trazon. *Biochemical Pharmacology*, 63(8):1465–1470.
- Tadolini B. 1987a. Iron autoxidation in Mops and Hepes buffers. *Free Radical Research Communications*, 4(3):149–160.
- Tadolini B. 1987b. Iron oxidation in Mops buffer. Effect of EDTA, hydrogen peroxide and FeCl₃. *Free Radical Research Communications*, 4(3):173–182.
- Tadolini B, Sechi AM. 1987. Iron oxidation in Mops buffer. Effect of phosphorus containing compounds. *Free Radical Research Communications*, 4(3):161–172.
- Tang YQ, Dong YX, Vennerstrom JL. 2004. Synthetic peroxides as antimalarials. *Medicinal Research Reviews*, 24(4):425–448.
- Torres-Guerrero E, Arenas R, Quintanilla-Cedillo MR, Ruiz-Esmenjaud J. 2017. Leishmaniasis: A review. *F1000Research*, 6:750.
- Trudell JR. 1987. Ethyl acetate extraction of spin-trapped free radicals: A reevaluation. *Free Radical Biology & Medicine*, 3:133–136.
- Våtsveen TK, Myhre MR, Steen CB, Wälchli S, Lingjærde OC, Bai B, Dillard P, Theodossiou TA, Holien T, Sundan A, et al. 2018. Artesunate shows potent anti-tumor activity in B-cell lymphoma. *Journal of Hematology & Oncology*, 11:23.
- Veber DF, Johnson SR, Cheng HY, Smith BR, Ward KW, Kopple KD. 2002. Molecular properties that influence the oral bioavailability of drug candidates. *Journal of Medicinal Chemistry*, 45(12):2615–2623.
- Venkataraman S, Schafer FQ, Buettner GR. 2004. Detection of lipid radicals using EPR. *Antioxidants & Redox Signaling*, 6(3):631–638.
- Wang J, Zhang CJ, Chia WN, Loh CC, Li Z, Lee YM, He Y, Yuan LX, Lim TK, Liu M, et al. 2015. Haem-activated promiscuous targeting of artemisinin in *Plasmodium falciparum*. *Nature Communications*, 6:10111.
- Weber RT. 2011. *XenonUsersGuide*. MA USA: Billerica. 336.
- Wheeler RJ, Gluenz E, Gull K. 2011. The cell cycle of *Leishmania*: Morphogenetic events

and their implications for parasite biology. *Molecular Microbiology*, 79(3):647–662.

World Health Organization. 2018. Endemicity of Leishmaniasis 2018. [Internet] Switzerland: World Health Organization, [cited 2020 march 22]. Available from: <https://www.who.int/leishmaniasis/burden/en/>.

World Health Organization. 2019. Interregional meeting on leishmaniasis among neighbouring endemic countries in the Eastern Mediterranean, African and European regions. Document WHO-EM/CTD/081/E, 47.

Yin H, Xu L, Porter NA. 2011. Free radical lipid peroxidation: Mechanisms and analysis. *Chemical Reviews*, 111:5944–5972.

Zulfiqar B, Shelper TB, Avery VM. 2017. Leishmaniasis drug discovery: Recent progress and challenges in assay development. *Drug Discovery Today*, 22(10):1516–1531.

9. List of figures

Fig. 1: Lifecycle of <i>Leishmania</i> parasites.	3
Fig. 2: Worldwide distribution of cases of visceral leishmaniasis in 2018.	5
Fig. 3: Activation of artemisinin (Art) in <i>Plasmodium falciparum</i>	13
Fig. 4: Formation of primary and secondary radicals upon EP activation.	14
Fig. 5: Principle of EPR spectroscopy.....	15
Fig. 6: Typical reactions of 5,5-dimethyl-1-pyrroline N-oxide (DMPO) and 2-methyl-2-nitrosopropane (MNP) with radicals.	17
Fig. 7: Structure of commonly used spin traps..	18
Fig. 8: Dose response curve of the viability of LtP as a function of different concentrations of Art.....	30
Fig. 9: EPR spectrum recorded after 3 min incubation of H ₂ O ₂ with FeSO ₄ in the presence of DMPO in H ₂ O at room temperature.	32
Fig. 10: EPR spectrum recorded after incubation of 472 μM H ₂ O ₂ with 94 μM FeSO ₄ in the presence of 42 mM DMPO in water and the corresponding simulated spectrum generated with the WINSIM software.....	33
Fig. 11: Time- and concentration-dependent development of the DMPO/•OH adduct intensity (I _{pp}) in 200 μL water with 42 mM DMPO, 472 μM H ₂ O ₂ and different concentrations of FeSO ₄	34
Fig. 12: Detected intensity (I _{pp}) of the DMPO/•OH adduct 3 min after mixing (t _{EPR} = 0) in 200 μL water with 42 mM DMPO, 472 μM H ₂ O ₂ and different concentrations of FeSO ₄	34
Fig. 13: Slope of the DMPO/•OH intensity over the first three minutes (t _{EPR} = 0, 1, 2 min)....	35
Fig. 14: Time- and concentration-dependent development of the DMPO/•OH adduct intensity (I _{pp}) in 200 μL PBS with 39 mM DMPO, 439 μM H ₂ O ₂ and different concentrations of FeSO ₄	36
Fig. 15: EPR spectrum recorded after 3 min incubation of Asc with FeSO ₄ in the presence of DMPO in water.	37
Fig. 16: EPR spectrum recorded after incubation of 439 μM Asc with 439 μM FeSO ₄ in the presence of 39 mM DMPO in water and the corresponding simulated spectrum generated with the WINSIM software.....	38
Fig. 17: Time- and concentration-dependent development of the DMPO/•C adduct intensity (I _{pp}) in 200 μL water with 39 mM DMPO, 439 μM Asc and different concentrations of FeSO ₄	39

Fig. 18: Time- and concentration-dependent development of the DMPO/•OH adduct intensity (Ipp) in 200 µL water with 39 mM DMPO, 439 µM Asc and different concentrations of FeSO ₄	39
Fig. 19: EPR spectrum obtained after 3 min incubation of Asc (346 µM) with FeSO ₄ (1384 µM) in 200 µL PBS in the presence of DMPO (31 mM).....	40
Fig. 20: EPR spectrum recorded after incubation of 346 µM Asc with 1384 µM FeSO ₄ in the presence of 31 mM DMPO in PBS and the corresponding simulated spectrum generated with the WINSIM software.....	41
Fig. 21: Time- and concentration-dependent development of the DMPO/•C adduct intensity (Ipp) in 200 µL PBS upon incubation of 31 mM DMPO with 346 µM Asc and different concentrations of FeSO ₄	42
Fig. 22: EPR spectrum recorded after incubation of 497 µM Art with 1086 µM FeSO ₄ in the presence of 39 mM DMPO in water and the corresponding simulated spectrum generated with the WINSIM software.....	43
Fig. 23: EPR spectrum recorded after incubation of 1100 µM FeSO ₄ with 39 mM DMPO in water and the corresponding simulated spectrum generated with the WINSIM software.....	44
Fig. 24: Time-dependent development of the DMPO/•C and DMPO/•OH adduct intensities (Ipp) in 200 µL water with 39 mM DMPO, 497 µM Art and 1086 µM FeSO ₄	45
Fig. 25: Time-dependent development of the DMPO/•C and DMPO/•OH adduct intensities (Ipp) in 200 µL water with 39 mM DMPO and 1100 µM FeSO ₄	45
Fig. 26: Time-dependent development of the DMPO/•C and DMPO/•OH adduct intensities (Ipp) in 200 µL PBS with 39 mM DMPO, 497 µM Art and 1086 µM FeSO ₄	46
Fig. 27: Time-dependent development of the DMPO/•C and DMPO/•OH adduct intensities (Ipp) in 200 µL PBS with 39 mM DMPO and 1100 µM FeSO ₄	46
Fig. 28: EPR spectrum recorded after incubation of 599 µM Asc with 2 * 10 ⁹ LtP/mL in the presence of 40 mM DMPO in PBS/Glucose (15 mM) and the corresponding simulated spectrum generated with the WINSIM software.....	47
Fig. 29: EPR spectrum recorded after incubation of 599 µM Asc with 4 * 10 ⁹ LtP/mL in the presence of 40 mM DMPO in PBS/Glucose (15 mM) and the corresponding simulated spectrum generated with the WINSIM software.....	48
Fig. 30: Time-dependent development of the DMPO/•C and DMPO/•OH adduct intensities (Ipp) in 200 µL PBS/Glucose (15 mM) with 2*10 ⁹ LtP/mL, 40 mM DMPO and 599 µM Asc..	49

Fig. 31: Time-dependent development of the DMPO/•C and DMPO/•OH adduct intensities (Ipp) in 200 µL PBS/Glucose (15 mM) with $2 \cdot 10^9$ LtP/mL and 40 mM DMPO..	49
Fig. 32: Time-dependent development of the DMPO/•C and DMPO/•OH adduct intensities (Ipp) in 200 µL PBS/Glucose (15 mM) with $4 \cdot 10^9$ LtP/mL, 40 mM DMPO and 599 µM Asc..	50
Fig. 33: Time-dependent development of the DMPO/•C and DMPO/•OH adduct intensities (Ipp) in 200 µL PBS/Glucose (15 mM) with $4 \cdot 10^9$ LtP/mL and 40 mM DMPO..	50
Fig. 34: Time-dependent development of the DMPO/•C and DMPO/•OH adduct intensities (Ipp) in 200 µL PBS/Glucose (15 mM) with $2 \cdot 10^9$ LtP/mL, 40 mM DMPO and 756 µM Art..	51
Fig. 35: Time-dependent development of the DMPO/•C and DMPO/•OH adduct intensities (Ipp) in 200 µL PBS/Glucose (15 mM) with $2 \cdot 10^9$ LtP/mL and 40 mM DMPO..	52

10. List of tables

Tab. 1: The most relevant species of human-pathogenic <i>Leishmania</i> and corresponding clinical manifestations.....	2
Tab. 2: Total concentrations for selected metals in LtP and J774 cells	11
Tab. 3: Iron concentrations in LtP	12
Tab. 4: Iron concentrations in J774 cells.....	12
Tab. 5: Bioavailability parameters of spin traps generated with the software BIOVIA Draw..	18
Tab. 6: EPR signals detected for endoperoxides in chemical (Fe^{2+}) and biological (LtP) systems..	21
Tab. 7: List of chemicals and suppliers used for this study.....	23
Tab. 8: IC_{50} values of antileishmanial compounds and spin traps..	31
Tab. 9 IC_{50} values of antileishmanial compounds in the presence or absence of the spin trap DMPO and its influence on the viability of LtP.....	31
Tab. 10: EPR spectra of extracted lipophilic DMPO spin adducts in LtP with Asc and without Asc, in model systems (LA) and control samples in PBS/Glucose..	53
Tab. 11: EPR spectra of extracted lipophilic DMPO spin adducts in LtP with Asc and without Asc and in control samples without LtP.....	54
Tab. 12: EPR spectra of extracted lipophilic DMPO spin adducts in LtP with Asc, without Asc and in control samples without LtP.	55
Tab. 13: Control experiment in PBS or PBS/Glucose with DMPO and comparison of chloroform (CHCl_3) and dichloromethane (CH_2Cl_2)..	56
Tab. 14: Control experiment in PBS with and without DMPO.....	57
Tab. 15: Coupling constants (a_N , $a_H(\beta)$, $a_H(\gamma)$) of DMPO spin adducts in ethyl acetate	62